

Analysis of Processes with Axisymmetric Plastic Flow of Metals

M.A. Zapara, N.D. Tutyshkin, W.H. Müller, R. Wille

A numerical method for the analysis of stresses and plastic flow rates is presented for processes with axisymmetric plastic flow of metals. This technique is based on a representation of yield zones in a special formulation of the stresses related to Iljushin's deviatoric stress space. The basic differential equations describing axisymmetric plastic flow are solved by hyperbolic approximations. In fact, the approach represents an enhanced method of slip lines since the characteristics of the differential equations for stresses and rates coincide with these. This condition is very important for the analysis of damage induced by voids which generate microscopic slip bands. The method is illustrated by an analysis of the forging process of an axisymmetric part made of low-carbon low-alloy steel. The stepwise analysis of deformation allows for calculating the contact load applied to the working tool, the strains accumulated within the part volume, and some "meso-parameters," e.g., the damage induced by strain micro-defects and the internal energy of hardening. Two integral measures connected with the hydrostatic and deviatoric parts of the damage tensor are used for the calculation of strain-induced damage. The predicted damage is significantly less than its permissible value, as high hydrostatic pressure in the plastic zone heals micro-defects, prevents their growth, and, thereby, increases the processing ductility of deformed metals during forging. The research results allow us to give some recommendations for the selection of appropriate processing strains for forging in order to achieve high strength properties of the produced axisymmetric case-shaped parts.

1 Introduction

Products of complex axisymmetric shape and high operational properties are widely used in Metal Forming (MF) technologies. Methods of applied plasticity theory are used for developing the manufacturing processes. These methods allow to calculate stress and strain fields and the related technological parameters for preset conditions as well as to predict structural and mechanical properties of the finished product material. A reliable determination of the Stress-Strain State (SSS) in MF processes becomes especially important when studying a volume distribution of strains, mechanical properties, as well as damage induced by micro-defects in order to predict the limit state of the workpiece material. For example, the limit state in the intense strain zones essentially depends on the history of deformation, stress triaxiality, and the local heat generation related to the dissipated energy of plastic deformation. All of this indicates that a problem of reliable determination of the SSS is still an ongoing topic for MF techniques.

State-of-the-art Finite Element (FE) codes successfully solve technological problems of MF. They create huge and constantly increasing opportunities of numerical modeling of deformation. However, if a more in-depth understanding of MF operations is required methods closely related to the physical behavior of plastic deformation are advantageous. Such a technique is the slip line method which is used for studying processes with plane plastic flow (Hill, 1950). Application of this method to the analysis of processes with axisymmetric deformation is reasonable from a scientifically-cognitive point of view, for example, for an investigation of strain induced damage. It is experimentally established that large defects (voids) generate microscopic slip bands (Yokobori, 1968). Therefore, a determination of slip line (band) fields is necessary for the prediction of damage and of the limit state of the material before its macro-destruction. Actually, the approach developed by the authors can be considered as the slip line method modernized for the analysis of the SSS and related structural and mechanical parameters in processes with axisymmetric flow.

It is known that the system of the fundamental equations describing axisymmetric plastic deformation is locally statically indetermined as only three equations for the stresses are available but four nonzero components of the stress tensor exist, namely two differential equilibrium equations and the plasticity condition (*cf.*, Kachanov, 2004). As a result there is a problem of determination the interconnected stress and velocity fields for preset forming conditions. The method for solving this problem suggested here is based on yield zone mapping in a

special representation stress space related to A.A. Iljushin's stress deviator concept (Iljushin, 1963). This space allows us to find an initial approximate solution in stresses and velocities using a "flexible" additional condition for the normalized deviator. The subsequent exact solution of the arising boundary problems is found by the method of hyperbolic approximations.

The correct information on stress and velocity fields for different stages of the studied forming process is then used for calculating technological parameters and for solving the kinetic equations for the structural and mechanical parameters of the processed material. Our approach is especially important for modeling processes with large deformation, *e.g.*, forging, which is widely used in metal forming, as well as for a reliable prediction of the structural damage of deformed materials. The compressive regime of the stress state during forging promotes high ductility of the processed materials and, accordingly, a greater operational deformation. Therefore, forging provides high strength properties of products due to strain hardening. However, the factor that limits admissible deformation is clearly a very high pressure on the working tool. The components manufactured by cold forging are widely used in aerospace, motor car, and power engineering industry.

Because of the outlined difficulties many complicated problems in research and development of MF techniques can only insufficiently be investigated for products with irregular shape. In particular, for forging, where the processed material is under complex loading with strong variations of the stress state, it is very difficult to analyze and optimize the full process. In this context, forging requires thorough research and modeling. Here we present a new solution method for the analysis of typical axisymmetric MF processes. The underlying equations and their solution will be described in the next two sections. It should be emphasized that we construct the fundamental solution in stresses and velocities concurrently and an iterative scheme yields an almost exact solution. For solvability it is temporarily necessary to modify the basic equations so that they become a determinate system, separately in stresses and in velocities. Such an additional condition is formulated in Section 3 by means of the maximum shear stress trajectories in characteristic cross-sections of the plastic zone. We conclude with the analysis of forging of a case-shaped part.

2 Fundamental equations for axisymmetric fields of stress and plastic flow velocities

Axisymmetric plastic flow of materials in MF processes can conveniently be described in a cylindrical coordinate system where r , z , θ denote the radial, the axial, and the circumferential direction, respectively. The deformed material is considered as a rigidly-plastic solid because plastic strains amount to 70–90% at MF being $\approx 10^2$ larger than elastic strains in metal forming processes (*e.g.*, drawing, die forging, extrusion). The calculation of the stress-strain state and related parameters of forming processes by using the model of rigid-plastic solid leads to quite satisfactory results corresponding to experimental data. The evolution of strain damage results in plastic dilatation. According to test data plastic dilatation of engineering materials does not exceed 2–5% even at large processing deformations. This fact enables one to make an assumption concerning the incompressibility of the material when determining the fields of plastic flow velocities. The basic equations of plasticity are given by the differential equations of equilibrium

$$\frac{\partial \sigma_r}{\partial r} + \frac{\partial \tau_{rz}}{\partial z} + \frac{\sigma_r - \sigma_\theta}{r} = 0, \quad \frac{\partial \tau_{rz}}{\partial r} + \frac{\partial \sigma_z}{\partial z} + \frac{\tau_{rz}}{r} = 0, \quad (1)$$

the von Mises yield surface

$$(\sigma_r - \sigma_z)^2 + (\sigma_z - \sigma_\theta)^2 + (\sigma_\theta - \sigma_r)^2 + 6\tau_{rz}^2 = 6\tau_y^2, \quad (2)$$

the condition of coaxiality of the strain rate deviator, \dot{e}_{ij} , and the stress deviator, s_{ij}

$$\frac{\partial v_r / \partial z + \partial v_z / \partial r}{2\tau_{rz}} = \frac{\partial v_r / \partial r - \partial v_z / \partial z}{\sigma_r - \sigma_z}, \quad (3)$$

the condition of similarity of the deviators \dot{e}_{ij} and s_{ij} (4), *i.e.*, of coincidence of their Lode angles, $\phi_{\dot{e}}$ and ϕ_σ (I_2 and I_3 being the second and third invariant of the corresponding symmetric tensors)

$$\sqrt{\frac{I_2(\dot{e}_{ij})}{I_2(s_{ij})}} = \sqrt[3]{\frac{I_3(\dot{e}_{ij})}{I_3(s_{ij})}}, \quad (4)$$

the incompressibility condition

$$\frac{\partial v_r}{\partial r} + \frac{\partial v_z}{\partial z} + \frac{v_r}{r} = 0, \quad (5)$$

and kinetic equations for parameters related to the meso-structure, μ_k

$$\frac{d\mu_k}{dt} = \dot{\mu}_k(\sigma_{ij}, T, \chi_s, \mu_k), \quad (6)$$

where $\sigma_r, \sigma_z, \sigma_\theta, \tau_{rz}$ are nonzero components of the stress tensor σ_{ij} , τ_y is the yield stress for shear, v_r and v_z are the components of the vector of plastic flow velocity, $I_2(\dot{e}_{ij}) = \dot{e}^2$, $I_3(\dot{e}_{ij})$, $I_2(s_{ij}) = s^2$, $I_3(s_{ij})$ are the second and the third invariant of deviatoric strain rates \dot{e}_{ij} and deviatoric stresses s_{ij} , respectively, \dot{e} , s denote the equivalent deviatoric strain rate and stress, μ_k are parameters of the meso-structure, e_{ij} are deviatoric strains, T is the thermodynamic temperature, χ_s are parameters connected with deviatoric strains e_{ij} , and t denotes time.

As physico-structural parameters μ_k we will specifically choose a micro-defect damage parameter ω , the grain size D of the polycrystal, and the energy characteristic $u^{(\mu)}$ of irreversible changes of the crystal lattice (*viz.*, a density of the internal energy of hardening, u_h). For the parameters χ_s , which are associated with the deformation, the intensity of shear strain rate, $\dot{\Lambda}$, and the cumulative shear strain, Λ , or Odquist parameter, are used

$$\dot{\Lambda} = \sqrt{2\dot{e}_j^i \dot{e}_i^j}, \quad \Lambda = \int_{s(t)} \sqrt{2\dot{e}_j^i \dot{e}_i^j} dt, \quad (7)$$

where \dot{e}_j^i denote the mixed components of the strain rate deviator. The parameters $\dot{\Lambda}$ and Λ are connected by the non-holonomic equation $d\Lambda/dt = \dot{\Lambda}$. For each strain path, $s(t)$, the parameter Λ can be determined by integration according to Eqn. (7) provided that strain rates \dot{e}_j^i are known.

The axisymmetric SSS has the following features. For the stress components we have $\tau_{z\theta} = \tau_{\theta r} = 0$, $v_\theta = 0$. The hoop stress σ_θ is a principal stress. Two special classes of plane problems follow from Eqns. (1)-(6): If the axial deformation vanishes in z -axis direction (*i.e.*, $e_z = 0$) Eqns. (1)-(6) describe a state of plain strain with circular boundaries. If the hoop strain vanishes, $e_\theta \rightarrow 0$, then, according to the flow rule, it follows for the hoop stress that $\sigma_\theta \rightarrow \langle \sigma \rangle = (\sigma_r + \sigma_z + \sigma_\theta)/3$, and Eqns. (1)-(6) describe plane flow in meridian cross-sections (with the normal n_θ) of the blank. The second special case can be applied to the analysis of deep-drawing of thin-walled axisymmetric shells. As is shown by Hill (1950), if the ratio between thickness, s , and diameter, d , of the shell is $s/d \leq 0.05$ then its deformation during deep-drawing is plane since the hoop stress σ_θ is infinitely small. In order to represent the axisymmetric SSS completely it will be sufficient to determine a field of stresses and flow velocities in one of the meridian cross-sections of the deformed solid.

For the analysis of axisymmetric MF processes with rapidly changing SSS we propose a method based on a concurrent construction of the initial approximate solution in stresses and velocities which is followed by an iterative process resulting in the exact solution. For solvability it is reasonable to temporarily modify Eqns. (1)-(6) so that they are written separately in stresses and in velocities, *e.g.*, by using additional conditions in terms of stresses. It allows us to transform the basic equations to a set of equations of the hyperbolic type with two sets of characteristics in a meridian cross-section of the deformed solid and to use some physical properties of slip lines. A similar approach was applied in the solution of axisymmetric problems by fixation of the Lode angle ϕ_σ . However, the

use of a “rigid” additional condition by fixing the Lode angle ϕ_σ for the initial approximate solution may contradict the condition (4). Therefore, the use of a “flexible” additional condition is to be preferred. It does not limit the phase of stresses and strain rates in the fundamental solution, *i.e.*, the Lode angle ϕ_σ , and it is more effective. Moreover, from the theoretical point of view an additional condition should be universal and invariant for the hydrostatic stress $\langle\sigma\rangle$, and it should allow us to recover known solutions as well as experimental results of processing problems. Such an additional condition can be formulated by means of differential geometry and will be described in detail in the following section.

3 Enhanced slip line method for axisymmetric deformation

The required additional condition can be formulated for the parameters that determine the differential geometry of slip lines in the meridian cross-sections of the plastic zone. Two mutually orthogonal directions, α and β , exist in each point of the meridian cross-section. Along these directions the tangential stresses $\tau_{\beta\alpha}$ and $\tau_{\alpha\beta}$ assume extreme values and the normal stresses are equal, *i.e.*, $\sigma_\alpha = \sigma_\beta$. The directions α and β form two families of mutually orthogonal lines in the meridian cross-section of plastic zone

$$\frac{dz}{dr} = \tan\delta_\theta \text{ (at line } \alpha \text{)}, \quad \frac{dz}{dr} = -\cot\delta_\theta \text{ (at line } \beta \text{)}, \quad (8)$$

where δ_θ is the angle between the r -axis and the line α . The angle δ_θ is connected with the stress components by the following relation:

$$\tan(2\delta_\theta) = -\frac{\sigma_r - \sigma_z}{2\tau_{rz}}, \quad (9)$$

which can be used in the initial approximate solution as the additional condition in terms of stresses.

It was shown by Tutyshkin *et al.* (2001) that the geometry of the slip lines strongly depends on the boundary conditions, *e.g.*, on the geometry and on the conditions of the contact surface of the working tools. This allows us to determine the function $\delta_\theta(r, z)$ in Eqns. (8) by known approximate solutions or by experimental determination of slip line trajectories. Slip line trajectories can be successfully found by experiments using the special technique for preparing a polished micro-section. An advantage of this technique is the possibility to detect slip line trajectories in any cross-section of test specimens without losing their continuity during deformation.

A comparison of the stress fields in the processes with axisymmetric and plane deformation indicates a geometric similarity of their slip line trajectories. This occurs when the boundary conditions are similar both in the meridian cross-section of the axisymmetric process and in the flow surface of the plane process (*e.g.*, when embedding conical and wedge punches, metal flow in convergent axisymmetric and wedge dies, compression (upsetting) of a thin layer). This property of trajectories α , β allows us to determine angle parameter $\delta_\theta^{(0)}$ in the initial approximate solution of problems for axisymmetric strain states by the solutions of corresponding problems for plane strain states, *i.e.*, to assume $\delta_\theta^{(0)}$ in the initial approximate solution as a known function of meridian coordinates $\delta_\theta(r, z)$

$$\delta_\theta^{(0)} = \frac{1}{2} \arctan\left(-\frac{\sigma_r - \sigma_z}{2\tau_{rz}}\right) = \delta_\theta(r, z). \quad (10)$$

The two differential equations of equilibrium (1), the yield condition (2), and the additional condition (10) form a local statically determinate system of equations for the four unknown stress components σ_r , σ_z , σ_θ , τ_{rz} . Thus the solution of the equations (1), (2), and (10) gives an admissible tensor field of stresses. In a geometrical interpretation the solution is mapped by the line M_1N_1 onto the von Mises yield surface in the principal stress space $\sigma_1, \sigma_2, \sigma_3$ (*cf.*, Figure 1).

The coaxiality condition (3) for the strain rate deviator $\dot{\epsilon}_{ij}$ and the stress deviator s_{ij} together with the incompressibility condition (5) form a closed system for the two unknown components v_r, v_z . Its solution allows us to define an admissible velocity field, and, in a geometrical interpretation, to find for each point of the plastic zone its graphic representation (line M_2N_2) onto the von Mises cylinder (*cf.*, Figure 1) by using the equations of plastic flow (Tutyshkin, 2005). The line MN corresponding to the exact solution is located between the line segments M_1N_1 and M_2N_2 . Therefore, a repetitive computational process leading to the exact solution can be interpreted as a mutual rotation of the generating lines M_1N_1 and M_2N_2 about the hydrostatic axis $\sigma_1 = \sigma_2 = \sigma_3$ until the coincidence condition (4) for the phases (*i.e.*, the Lode angles) of the deviators $\dot{\epsilon}_{ij}$ and s_{ij} is fulfilled with preset accuracy. Thus Eqn. (4) can be considered as a differential constraint to be satisfied by the exact solution. Hence, each plastic particle of the deformed material is mapped by a line moving on yield surface $f = 0$ under complex loading, *i.e.*, in case of the generalized von Mises condition (2), onto the surface of the second invariant of the stress deviator s_{ij} .

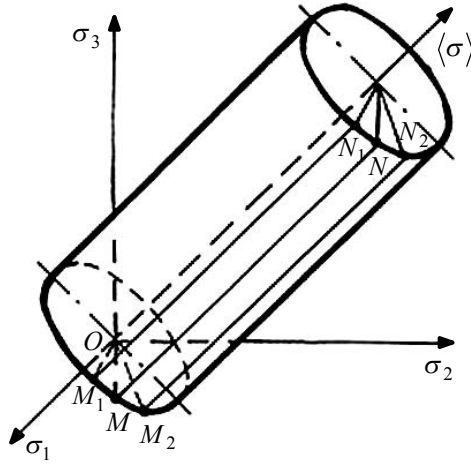


Figure 1. Representation of the solution for the components σ_{ij}, v_i in principal stress space $\sigma_1, \sigma_2, \sigma_3$.

A similar type of deformation process corresponds to local strain theory (Malmeisters *et al.*, 1980) where the strain is considered to be the result of elementary deformation mechanisms (sliding, twinning) in the discrete polycrystalline structure. Malmeyster *et al.* (1980) introduced a probability factor F_s^+ / F_s of plastic strain appearance in a spherical particle, where F_s^+ is a set of orientations of elementary slide areas, and F_s the area of the unit sphere. An experimentally defined increment of the factor F_s^+ / F_s can be represented as a segment of the generating line moving on the load surface ($f = 0$). Hence, the method proposed for determination of stress and velocity fields corresponds to the experimentally verified concept of the onset and evolution of plastic yield at a segment of the generating line “sliding” on the load surface ($f = 0$).

From this viewpoint the advantage of cylindrical surfaces selected as the load surface, $f = 0$, described by the von Mises function becomes obvious. The movement of a segment of the generating line under complex loading can be interpreted as its rotation about the hydrostatic axis $\sigma_1 = \sigma_2 = \sigma_3$ in principal stress space $\sigma_1, \sigma_2, \sigma_3$, *i.e.*, as a change in the Lode angles of the stress and the strain rate deviators s_{ij} and $\dot{\epsilon}_{ij}$, respectively.

When solving the constitutive equations (1)-(6) it is convenient to set a position of a segment of the generating line (MN) on the load surface in a special representing space of the parameters $\varphi_\theta, m_\theta, m_r, m_z$ which are introduced by the following relations

$$\tan(2\varphi_\theta) = \sqrt{\frac{2}{3}} \tan(2\delta_\theta), \quad (11)$$

$$sm_\theta \cos(2\varphi_\theta) = \tau_{\alpha\beta} \cos(2\delta_\theta), \quad (12)$$

$$I_1(\bar{s}_{ij}) = m_\theta \sin 2\varphi_\theta - m_r \text{sign}(\sigma_z - \sigma_\theta) - m_z \text{sign}(\sigma_\theta - \sigma_r) = 0, \quad (13)$$

$$I_2(\bar{s}_{ij}) = m_\theta^2 + m_r^2 + m_z^2 = 1, \quad (14)$$

where $I_1(\bar{s}_{ij})=0$, $I_2(\bar{s}_{ij})=1$ are the first and the second invariants of the normalized stress deviator $\bar{s}_{ij} = s_{ij} / \sqrt{I_2(s_{ij})} \equiv s_{ij} / s$, and $\text{sign}(\sigma_z - \sigma_\theta)$, $\text{sign}(\sigma_\theta - \sigma_r)$ are the sign functions, *i.e.*, the signs of the arguments $(\sigma_z - \sigma_\theta)$ and $(\sigma_\theta - \sigma_r)$.

The representing space of the parameters φ_θ , m_θ , m_r , m_z is connected with Iljushin's deviatoric space (Iljushin, 1963)

$$\begin{aligned} \bar{s}_1 \cos \beta_\sigma + \bar{s}_2 \sin \beta_\sigma &= -m_z \text{sign}(\sigma_\theta - \sigma_r) - m_\theta \sin(2\varphi_\theta), \\ -\bar{s}_1 \sin\left(\beta_\sigma + \frac{\pi}{6}\right) + \bar{s}_2 \cos\left(\beta_\sigma + \frac{\pi}{6}\right) &= m_\theta \sin(2\varphi_\theta) + m_r \text{sign}(\sigma_z - \sigma_\theta), \\ \bar{s}_1 \sin\left(\beta_\sigma - \frac{\pi}{6}\right) - \bar{s}_2 \cos\left(\beta_\sigma - \frac{\pi}{6}\right) &= -m_r \text{sign}(\sigma_z - \sigma_\theta) + m_z \text{sign}(\sigma_\theta - \sigma_r), \\ \frac{\bar{s}_3}{\sqrt{2}} = m_\theta \cos(2\varphi_\theta), \quad \frac{\bar{s}_4}{\sqrt{2}} = 0, \quad \frac{\bar{s}_5}{\sqrt{2}} = 0, \end{aligned} \quad (15)$$

where \bar{s}_i ($i=1,2,\dots,5$) are the components of the five-dimensional vector s with the scalar $|s| = \sqrt{I_2(\bar{s}_{ij})} = 1$, and β_σ is the phase parameter of the stress deviator \bar{s}_{ij} . The deviatoric stresses $s_{ij} / s = \bar{s}_{ij}$ and the components of the five-dimensional vector s are connected by the following dependencies (Iljushin, 1963)

$$\begin{aligned} \bar{s}_r \sqrt{\frac{3}{2}} &= \bar{s}_1 \cos \beta_\sigma + \bar{s}_2 \sin \beta_\sigma, \quad \bar{s}_z \sqrt{\frac{3}{2}} = -\bar{s}_1 \sin\left(\beta_\sigma + \frac{\pi}{6}\right) + \bar{s}_2 \cos\left(\beta_\sigma + \frac{\pi}{6}\right), \\ \bar{s}_\theta \sqrt{\frac{3}{2}} &= \bar{s}_1 \sin\left(\beta_\sigma - \frac{\pi}{6}\right) - \bar{s}_2 \cos\left(\beta_\sigma - \frac{\pi}{6}\right), \quad \bar{s}_{rz} \sqrt{\frac{3}{2}} \equiv \bar{\tau}_{rz} \sqrt{\frac{3}{2}} = \bar{s}_3 \cos \frac{\pi}{6}, \\ \bar{s}_{z\theta} \sqrt{\frac{3}{2}} &\equiv \bar{\tau}_{z\theta} \sqrt{\frac{3}{2}} = \bar{s}_4 \cos \frac{\pi}{6} = 0, \quad \bar{s}_{\theta r} \sqrt{\frac{3}{2}} \equiv \bar{\tau}_{\theta r} = \bar{s}_5 \cos \frac{\pi}{6} = 0. \end{aligned} \quad (16)$$

The dependences of the tensorial stresses σ_{ij} on the parameters φ_θ , m_θ , m_r , m_z can be found from Eqns. (15) and (16)

$$\begin{aligned} \sigma_r &= \langle \sigma \rangle + \sqrt{\frac{2}{3}} \tau_y [-m_z \text{sign}(\sigma_\theta - \sigma_r) - m_\theta \sin(2\varphi_\theta)], \quad \sigma_z = \langle \sigma \rangle + \sqrt{\frac{2}{3}} \tau_y [m_\theta \sin(2\varphi_\theta) + m_r \text{sign}(\sigma_z - \sigma_\theta)], \\ \sigma_\theta &= \langle \sigma \rangle + \sqrt{\frac{2}{3}} \tau_y [-m_r \text{sign}(\sigma_z - \sigma_\theta) + m_z \text{sign}(\sigma_\theta - \sigma_r)], \quad \tau_{rz} = \tau_y m_\theta \cos(2\varphi_\theta). \end{aligned} \quad (17)$$

Note that the parametric representation (17) of the stress components corresponds to the invariants (13) and (14) of the normalized stress deviator \bar{s}_{ij} . Eqns. (17) together with Eqns. (13) and (14) allows us to determine the stress tensor σ_{ij} during axisymmetric deformation by using four quantities, the hydrostatic stress $\langle \sigma \rangle$, the yield stress τ_y , and the parameters φ_θ and m_θ (instead of the components σ_r , σ_z , σ_θ , τ_{rz}).

The sign functions $\text{sign}(\sigma_z - \sigma_\theta)$ and $\text{sign}(\sigma_\theta - \sigma_r)$ that appear in Eqns. (17) depend on the type of processing operations. In processes with predominant axial compression (*e.g.*, extrusion, upsetting, bulk forging) we have

$\sigma_r \geq \sigma_\theta \geq \sigma_z$, $\text{sign}(\sigma_z - \sigma_\theta) = -1$, $\text{sign}(\sigma_\theta - \sigma_r) = -1$;
 in processes with predominant axial tension (e.g., drawing, dragging)
 $\sigma_z \geq \sigma_\theta \geq \sigma_r$, $\text{sign}(\sigma_z - \sigma_\theta) = 1$, $\text{sign}(\sigma_\theta - \sigma_r) = 1$;
 in processes of expansion
 $\sigma_\theta \geq \sigma_z \geq \sigma_r$; $\text{sign}(\sigma_z - \sigma_\theta) = -1$, $\text{sign}(\sigma_\theta - \sigma_r) = 1$;
 in processes of pressing
 $\sigma_r \geq \sigma_z \geq \sigma_\theta$, $\text{sign}(\sigma_z - \sigma_\theta) = 1$, $\text{sign}(\sigma_\theta - \sigma_r) = -1$.

It is convenient to use a graphic presentation of the SSS for the analysis of plastic flow processes. The parametric representation for the stresses (17) allows us to graphically represent the normalized deviator in three-dimensional parametric space m_θ , m_r , m_z for the region $0 \leq m_\theta, m_r, m_z \leq 1$ (cf., Figure 2).

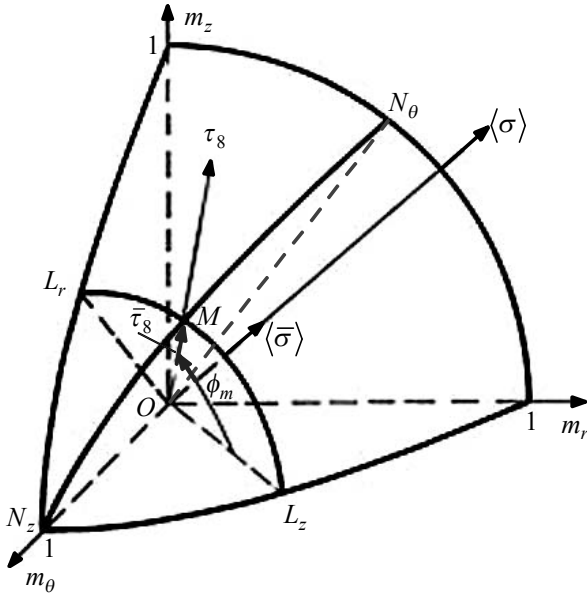


Figure 2. Graphic presentation of the stress deviator $s_{ij}/s = \bar{s}_{ij}$ at the axisymmetric stress state.

Eqn. (13) defines the deviatoric plane $I_1(\bar{s}_{ij}) = 0$ which passes through the point O and can be presented in the following form: $A_\theta m_\theta + A_r m_r + A_z m_z = 0$, where all the coefficients A_θ , A_r , A_z cannot be of equal signs. Eqn. (14) is equivalent to the yield condition (2) and determines the spherical surface $m_\theta^2 + m_r^2 + m_z^2 = 1$ (of unit radius $R = 1$) in the region $m_\theta, m_r, m_z \in [0;1]$. The intersection of the surfaces $I_1(\bar{s}_{ij}) = 0$ and $I_2(\bar{s}_{ij}) = 1$ defines the deviatoric curve $L_r L_z$ (cf., Figure 2). The third invariant $I_3(\bar{s}_{ij}) = \det \|\bar{\sigma}_{.j}^i - \bar{\sigma} \delta_{ij}\| = -2 \cos \phi_\sigma / 3\sqrt{3}$ is represented by a hyperboloid with the hydrostatic axis $\langle \bar{\sigma} \rangle = \langle \sigma \rangle / s$. The intersection of the surfaces $I_3(\bar{s}_{ij}) = -2 \cos \phi_\sigma / 3\sqrt{3}$ and $I_2(\bar{s}_{ij}) = 1$ defines the phase curve $N_z N_\theta$ of stresses. Moreover, the intersection of the curves $L_r L_z$ and $N_z N_\theta$ fixes the point $M(\varphi_\theta, m_\theta, m_r, m_z)$ which determines the vector of hydrostatic shear stress $\tau_8/s = \bar{\tau}_8$.

Physically speaking the parameters m_θ , m_r , m_z define a direction of the vector τ_8 in the deviatoric plane (13). We assume that $\text{sign}(A)_r = \text{sign}(A_\theta) = -\text{sign}(A_z)$. In this case the boundary points L_r and L_z of the deviatoric curve $L_r L_z$ are always in planes $m_r = 0$ and $m_z = 0$ for all possible combinations of stresses. The point L_r corresponds to uniaxial tension while the point L_z corresponds to uniaxial compression. The angle ϕ_m between the segments OL_z and OM is a representation of the Lode angle ϕ_σ in the parametric space m_θ, m_r, m_z .

Eqns. (1), (13), and (14) together with the parametric representation of stresses (17) takes the following form in

the system of coordinates α and β

$$\begin{aligned} \frac{\partial \langle \sigma \rangle}{\partial s_\alpha} + \sqrt{\frac{2}{3}} \tau_y \left[-\text{sign}(\sigma_\theta - \sigma_\alpha) \frac{\partial m_\beta}{\partial s_\alpha} - 2m_\theta \frac{\partial \varphi_\theta}{\partial s_\alpha} \right] - 2\tau_y m_\theta \frac{\partial \delta_\theta}{\partial s_\alpha} + \tau_y \frac{\partial m_\theta}{\partial s_\beta} - \\ - \sqrt{6} \tau_y \frac{m_\alpha}{r} \cos \delta_\theta \text{sign}(\sigma_\theta - \sigma_\alpha) - \tau_y \frac{m_\theta}{r} \sin \delta_\theta - \sqrt{\frac{2}{3}} m_\beta \text{sign}(\sigma_\theta - \sigma_\alpha) \frac{\partial \tau_y}{\partial s_\alpha} + m_\theta \frac{\partial \tau_y}{\partial s_\beta} = 0, \end{aligned} \quad (18)$$

$$\begin{aligned} \frac{\partial \langle \sigma \rangle}{\partial s_\beta} + \sqrt{\frac{2}{3}} \tau_y \left[2m_\theta \frac{\partial \varphi_\theta}{\partial s_\beta} + \text{sign}(\sigma_\beta - \sigma_\theta) \frac{\partial m_\alpha}{\partial s_\beta} \right] + 2\tau_y m_\theta \frac{\partial \delta_\theta}{\partial s_\beta} + \tau_y \frac{\partial m_\theta}{\partial s_\alpha} - \\ - \sqrt{6} \tau_y \frac{m_\beta}{r} \sin \delta_\theta \text{sign}(\sigma_\beta - \sigma_\theta) + \tau_y \frac{m_\theta}{r} \cos \delta_\theta + \sqrt{\frac{2}{3}} m_\alpha \text{sign}(\sigma_\beta - \sigma_\theta) \frac{\partial \tau_y}{\partial s_\beta} + m_\theta \frac{\partial \tau_y}{\partial s_\alpha} = 0, \end{aligned} \quad (19)$$

$$-m_\alpha \text{sign}(\sigma_\beta - \sigma_\theta) - m_\beta \text{sign}(\sigma_\theta - \sigma_\alpha) = 0, \quad (20)$$

$$m_\alpha^2 + m_\beta^2 + m_\theta^2 = 1. \quad (21)$$

Eqns. (19) and (20) result in

$$m_\alpha = m_\beta = \frac{1}{\sqrt{2}} \sqrt{1 - m_\theta^2}. \quad (22)$$

The angle δ_θ and the parameter φ_θ appearing in Eqns. (18) and (19) are connected by (11). Deviation of the non-linear dependence (11) from the linear relation $\varphi_\theta = \delta_\theta$ (*cf.*, Figure 3, left) corresponds to a deviation of the dependence $\mu_{\dot{\varepsilon}} = \mu_{\dot{\varepsilon}}(\mu_\sigma)$ from the Levi-von Mises equations (*cf.*, Figure 3, right). In Figure 3 (right) $\mu_{\dot{\varepsilon}} = 2(\dot{\varepsilon}_2 - \dot{\varepsilon}_3)/(\varepsilon_1 - \dot{\varepsilon}_3) - 1$ and $\mu_\sigma = 2(\sigma_2 - \sigma_3)/(\sigma_1 - \sigma_3) - 1$ are the coefficients of the strain and of the stress state, respectively. The experimental dependence $\mu_{\dot{\varepsilon}} = \mu_{\dot{\varepsilon}}(\mu_\sigma)$ was obtained by classical tests by Taylor and Quinny (Hill, 1950).

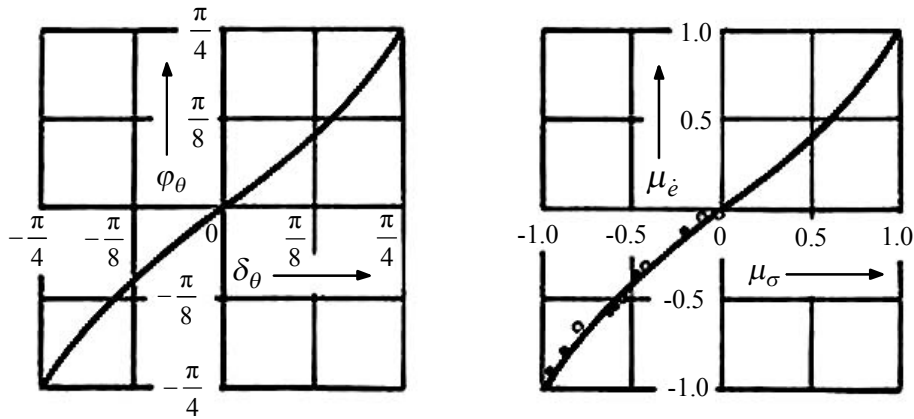


Figure 3. *left* - dependence $\varphi_\theta = \varphi_\theta(\delta_\theta)$, *right* - experimental dependence $\mu_{\dot{\varepsilon}} = \mu_{\dot{\varepsilon}}(\mu_\sigma)$,
 \circ – low-carbon steel, \bullet – copper

In view of the dependence (22) and the non-linear relation (11) between the parameters φ_θ and δ_θ , the differential equations (18) and (19) become

$$\frac{\partial \langle \sigma \rangle}{\partial s_\alpha} - 2\tau_y m_\theta \left[1 + \sqrt{\frac{2}{3}} \varphi'(\delta_\theta) \right] \frac{\partial \delta_\theta}{\partial s_\alpha} - \frac{\sqrt{1 - m_\theta^2}}{\sqrt{3}} \text{sign}(\sigma_\theta - \sigma_\alpha) \frac{\partial \tau_y}{\partial s_\alpha} + m_\theta \frac{\partial \tau_y}{\partial s_\beta} +$$

$$+ \tau_y \frac{m_\theta}{\sqrt{3}\sqrt{1-m_\theta^2}} \text{sign}(\sigma_\theta - \sigma_\alpha) \frac{\partial m_\theta}{\partial s_\alpha} + \tau_y \frac{\partial m_\theta}{\partial s_\beta} - \sqrt{3} \frac{\tau_y}{r} \sqrt{1-m_\theta^2} \cos \delta_\theta \text{sign}(\sigma_\theta - \sigma_\alpha) - \tau_y \frac{m_\theta}{r} \sin \delta_\theta = 0, \quad (23)$$

$$\begin{aligned} & \frac{\partial \langle \sigma \rangle}{\partial s_\beta} + 2\tau_y m_\theta \left[1 + \sqrt{\frac{2}{3}} \varphi'(\delta_\theta) \right] \frac{\partial \delta_\theta}{\partial s_\beta} + m_\theta \frac{\partial \tau_y}{\partial s_\alpha} - \frac{\sqrt{1-m_\theta^2}}{\sqrt{3}} \text{sign}(\sigma_\theta - \sigma_\alpha) \frac{\partial \tau_y}{\partial s_\beta} + \\ & + \sqrt{3} \frac{\tau_y}{r} \sqrt{1-m_\theta^2} \sin \delta_\theta \text{sign}(\sigma_\theta - \sigma_\alpha) + \tau_y \frac{\partial m_\theta}{\partial s_\alpha} + \tau_y \frac{m_\theta}{\sqrt{3}\sqrt{1-m_\theta^2}} \text{sign}(\sigma_\theta - \sigma_\alpha) \frac{\partial m_\theta}{\partial s_\beta} + \tau_y \frac{m_\theta}{r} \cos \delta_\theta = 0, \quad (24) \end{aligned}$$

where $\varphi'_\theta(\delta_\theta) = d\varphi'_\theta/d\delta_\theta$.

The velocity equations (3) and (5) can be rewritten in terms of fixed coordinates α^* and β^* coinciding with trajectories α and β

$$\frac{\partial v_{\alpha^*}}{\partial s_\alpha} - v_{\beta^*} \frac{\partial \delta_\theta}{\partial s_\alpha} + \frac{v_{\alpha^*} \cos \delta_\theta - v_{\beta^*} \sin \delta_\theta}{r} = 0, \quad (25)$$

$$\frac{\partial v_{\beta^*}}{\partial s_\beta} + v_{\alpha^*} \frac{\partial \delta_\theta}{\partial s_\beta} + \frac{v_{\alpha^*} \cos \delta_\theta - v_{\beta^*} \sin \delta_\theta}{2r} = 0. \quad (26)$$

The solution of Eqns. (4), (23)-(26) should satisfy Cauchy-type boundary conditions. In case of the axisymmetric problem the Cauchy-type conditions are presented by boundary values of the required functions $\langle \sigma \rangle$, δ_θ , m_θ , v_{α^*} , v_{β^*} at the two-dimensional surface $\omega(\alpha^*, \beta^*) = 0$ in the space α^* , β^* . Thus, the boundary problem of axisymmetric plastic flow is reduced to the solution of basic equations in the plane $rz(\alpha^*, \beta^*)$ (cf., Figure 4).

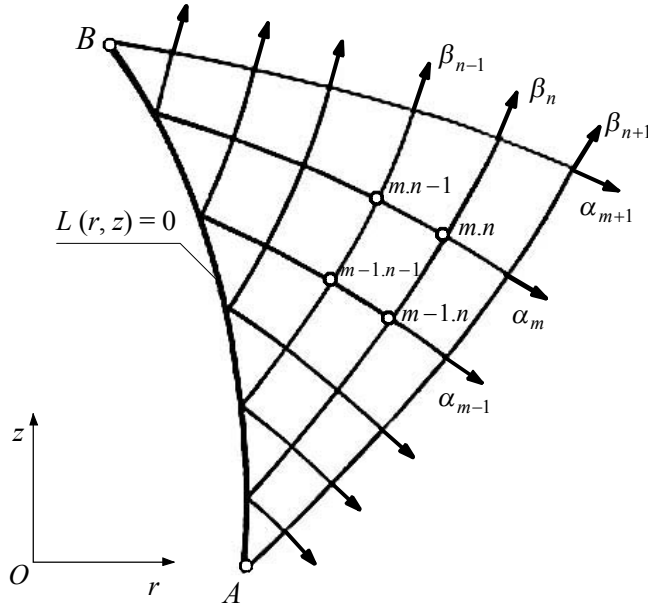


Figure 4. A boundary problem in the meridian plane rz at the axisymmetric plastic state.

The Eqns. (23) and (24) and the additional condition (10) form a locally definable set of the equations for three required components $\langle \sigma \rangle$, δ_θ , and m_θ . Two velocity relations (25) and (26) form a closed system for two required velocity components, v_{α^*} , v_{β^*} . The initial approximate solution of these sub-systems allows us to represent each node point of the plastic zone by two lines (M_1N_1 and M_2N_2) on the cylindrical yield surface in prin-

principal stress space $\sigma_1, \sigma_2, \sigma_3$ (*cf.*, Figure 1). One of these lines corresponds to admissible stresses, and the other to admissible velocities. The position of MN corresponding to the exact solution is situated between the lines M_1N_1 and M_2N_2 . The exact solution should satisfy the condition of coincidence of phases, *i.e.*, the Lode angles ϕ_ε and ϕ_σ , of the deviators $\dot{\varepsilon}_{ij}$ and s_{ij} (4).

The four partial differential equations (23)-(26) are closed w.r.t. five required functions $\langle \sigma \rangle, \delta_\theta, m_\theta, v_{\alpha^*}$ and v_{β^*} by means of the differential constraint (4). These four equations are of hyperbolic type and have two pairwise coincident sets of mutually orthogonal characteristics α and β . Characteristic lines α and β coincide with slip lines and are described by Eqns. (8). This fact allows us to use grid-characteristic schemes for the numerical solution of arising boundary problems.

The strain damage measures ω_1 and ω_2 connected with the second-rank order tensor of damage (ω_{ij}) are used as meso-structural parameters μ_k of the ductile material (*cf.*, Zapara *et al.*, 2008). The kinetic equation (6) for the damage measure ω_1 , which is related to plastic dilatation of the deformed material due to an increase in micro-defect volume, becomes

$$\frac{d\omega_1}{dt} = \frac{1}{\varepsilon_i^i(\Lambda_{lim})} \cdot \frac{d\varepsilon_i^i(\Lambda)}{d\Lambda} \cdot \frac{d\Lambda}{dt} \equiv \frac{[\varepsilon_i^i(\Lambda)]' \dot{\Lambda}}{\varepsilon_i^i(\Lambda_{lim})}, \quad (27)$$

where $\varepsilon_i^i(\Lambda)$ is plastic dilation ε_i^i (*i.e.*, the first invariant of the plastic strain tensor ε_{ij}) dependent on the cumulative strain at shear $\Lambda = \int_{s(t)} \sqrt{2\dot{\varepsilon}_j^i \dot{\varepsilon}_i^j} dt$, $\dot{\varepsilon}_j^i$ are the mixed components of the deviatoric strain, $s(t)$ is a load path, $\dot{\Lambda} = d\Lambda/dt$ is an intensity of the shear strain rate, and Λ_{lim} is the limit strain of the material at the moment of its macro-destruction.

The kinetic equation (6) for the damage measure ω_2 , which is connected with a change in micro-defect (void) shape under plastic deformation, takes on the following form

$$\frac{d\omega_2}{dt} = \frac{\hat{\varepsilon}}{\hat{\varepsilon}_{cr}} \equiv \frac{\sqrt{(1/2)(\hat{\varepsilon}_j^i \hat{\varepsilon}_i^j)}}{\hat{\varepsilon}_{cr}}, \quad (28)$$

where $\hat{\varepsilon}$ is the equivalent deviatoric strain rate of voids, $\hat{\varepsilon}_{cr}$ is the critical deviatoric strain of voids corresponding to a stage of intense coalescence of ellipsoidal voids and formation of cavernous defects, and $\hat{\varepsilon}_j^i$ are the mixed components of the deviatoric strain rate of voids.

Being described by differential equations the damage measures are defined over the following range: $\omega_1, \omega_2 \in [0;1]$, where the upper-range value $\omega_1=1$ corresponds to the moment of macro-fracture, and $\omega_2=1$ corresponds to the stage of formation of cavernous defects (*i.e.*, a stage of the micro-destruction at meso-scale).

4 Analysis of press forging of axisymmetric parts

4.1 Determination of consistent fields of stresses and plastic flow velocities

Press forging is used in the metalware engineering industry both independently and in combination with other forming operations. Products can be processed by press forging completely as well as partially. Powerful press equipment and high-strength tool steels allow us to apply Cold Press Forging (CPF) to manufacture a number of components for mechanical and aerospace engineering. Press forging operations relate to processes with non-stationary plastic flow which are very difficult to model (Dung, 1992). Various configurations of workpieces and complex boundary conditions result in heterogeneous and non-stationary fields of processing stresses, strains,

strain rates, mechanical and microstructural characteristics of deformed materials. Thus, the development and upgrading of manufacturing techniques including press forging is appreciably connected with the use of processing feasibilities of volumetric forming during these operations.

As a case study here we choose press forging of a small-height axisymmetric part with a flange when plastic flow spreads along all the height of a billet. We consider a final stage of press forging accompanied by the outflow of the metal into a radial clearance between the top die and the counter die (*cf.*, Figure 5). Figure 5 shows the meridian cross-section of the processed billet. The shape of the contact surface of the die is simplified. It can be complicated according to the shape of the finished part that will result in necessity of solving more complex boundary problems in order to determine a stress-strain state during press forging. The final stage of press forging is reached when the die cavity is filled up. It is accompanied by squeezing the metal into the radial clearance. The complete filling of the die cavity in press forging is accompanied by an increasing resistance to the metal outflow into the clearance. This deformation resistance should not abruptly increase in order to ensure high quality filling of the die cavity. The method given above will be used for the calculation of the mechanical properties and strain-induced damage of the material as well as for determination of pressure to be applied to the die.

All parameters of press forging are calculated using the following input data: The material of the part is an annealed low-carbon low-alloy steel (C 0.08-0.20 %, Cr 0.15-0.30 %) (*cf.*, Table 1); the diameter of the die cavity is given by $d_d=138$ mm (the diameter of the part is $d_p=d_d$, respectively), the height of the cylindrical billet at the beginning of press forging is $h_b=19.5$ mm while the height of the finished part is $h_p=14$ mm, the radial clearance h_c between the top die and the counter die changes during press forging from $h_{c0}=7$ mm to $h_{cf}=1.5$ mm. During the process we assume a constant processing speed with strain rates of $\dot{\epsilon}_i=10-100$ s⁻¹ and a given temperature of $T=300-500$ K. Note that this temperature is still below the recrystallization temperature of the steel.

The stress-strain state is evaluated at three stages (*cf.*, Figure 5), as follows

1. at the initial moment of the second stage when $\Delta h_1=0.60$ mm,
2. at an intermediate moment when $\Delta h_2=2.5$ mm,
3. at the final state, *i.e.*, $\Delta h_3=5.5$ mm,

where Δh_i denotes a displacement of the top die at a moment i , where $i=1-3$.

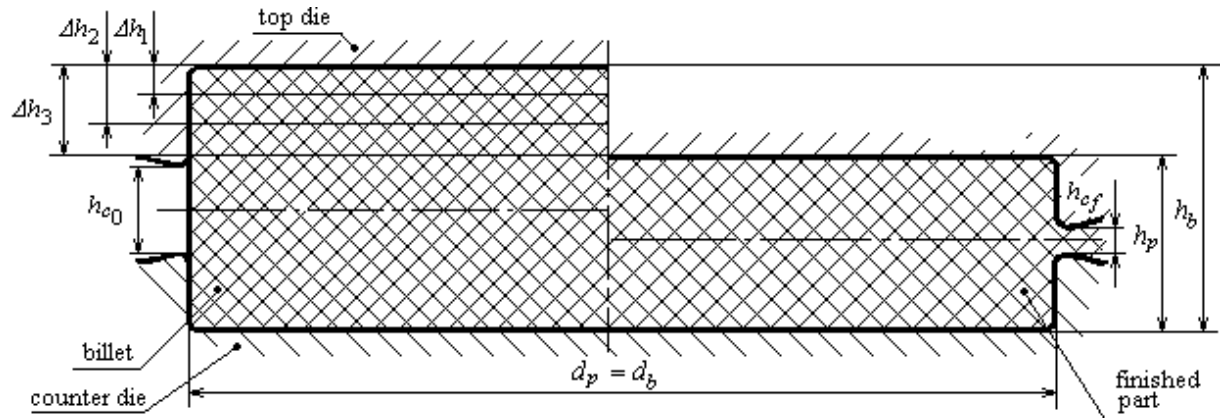


Figure 5. Press forging of an axisymmetric part

The yield stress under shear that appears in the von Mises function (2) can be written as $\tau_y = \sigma_y / \sqrt{3}$, where σ_y is the yield stress under uniaxial condition. This relation allows us to use uniaxial tension and compression tests in order to determine τ_y . As outlined in detail by Zapara *et al.* (2008) the evolution of the yield stress σ_y can be described by

$$\sigma_y = \sigma_y^{(is)} \exp \left[-\alpha \left(\frac{T - T_0}{T_{\max} - T_0} \right)^q \right], \quad (29)$$

where $\sigma_y^{(is)} = \sigma_y^{(is)}(e_i, \dot{e}_{i0}, T_0, \mu_k)$ refers to isothermal hardening curves obtained for various materials at a fixed strain rate \dot{e}_{i0} and an initial thermodynamic temperature T_0 , e_i is an intensity of the cumulative strains, μ_k are meso-structural parameters, T and T_{\max} are the current and the maximum temperature of the process, respectively, and α and q are parameters used in the equation for the temperature dependent yield strength σ_y (cf., Zapara *et al.*, 2008). The isothermal yield stress can be written as follows:

$$\sigma_y^{(is)} = \sigma_0 + \left(\sigma_{d/\omega=0} + A\omega^m \right) D^{-\frac{1}{2}l^{\frac{1}{2}}} + B e_i^{(n_0 - n_1 e_i)}, \quad (30)$$

where σ_0 is the initial yield stress given by the resistance to the movement of free dislocations, ω is the strain damage related to plastic dilatation induced by micro-defect growth, and σ_d is a stress required for the movement of locked dislocations which will be specified below. Moreover, A and m are parameters of the relationship $\sigma_d = \sigma_d(\omega)$, D is average grain size, l is a characteristic distance from the grain boundary to the nearest dislocation source, and B , n_0 , and n_1 are scalar parameters describing the work hardening of the yield stress in an isothermal regime.

Table 1. Parameters of plastically deformed low-carbon low-alloy steel (temperature $T = 300 - 500$ K, strain rate $\dot{e}_i = 10 - 100 \text{ s}^{-1}$)

σ_0 , MPa	$\sigma_{d/\omega=0}$, MPa	A , MPa	m	$l \cdot 10^{-2}$, mm	B , MPa	n_0	n_1	T_0 , K	T_{\max} , K	α	q
150	265	157	1.40	0.222	391	0.435	0.097	300	800	0.177	2.691

By substituting the data of Table 1 into Eqs. (4)-(5) we may determine the yield stress of this steel depending on strain hardening and micro-structural changes by

$$\sigma_y = \sigma_y^{(is)} \exp \left[-0.177 \left(\frac{T - 300}{500} \right)^{2.691} \right], \quad \sigma_y^{(is)} = 150 + 4.717 \cdot 10^{-2} \left(265 + 157 \omega^{1.40} \right) D^{-\frac{1}{2}} + 391 e_i^{(0.435 - 0.097 e_i)}. \quad (31)$$

Since the process characteristics depend on the strain history a stepwise analysis of deformation together with a detailed determination of stress-strain state is necessary for their calculation. For the purpose of the analysis the process of press forging will be divided into three stages since the plastic flow of the material is non-stationary.

First, we determine consistent fields of stresses and flow velocities at the moments corresponding to various displacements of the top die: $\Delta h_1 = 0.6$ mm, $\Delta h_2 = 2.5$ mm; $\Delta h_3 = 5.5$ mm. The following ratios of the changing dimensions correspond to these moments of press forging: $d_p/h_1 = d_p/(h_b - \Delta h_1) = 7.3$, $d_p/h_2 = d_p/(h_b - \Delta h_2) = 8.1$, and $d_p/h_3 = d_p/(h_b - \Delta h_3) = 9.9$. Shapes of the billet and the die as well as the contact conditions are mirrored w.r.t vertical and horizontal axes of symmetry. The fields of stresses, flow velocities, and strains are mirrored w.r.t these axes of symmetry as well. Therefore, in order to present the figures more compactly and with enough large scale we shall show in this paper only one fourth of the fields of stresses and flow velocities (to the left and above the axes of symmetry, cf., Figures 7, 9, 11, 12).

By solving the boundary problem we may construct a field of slip lines (*i.e.*, characteristics) in the meridian cross-section of the axisymmetrically deformed material. (Details of the employed numerical scheme are summarized in the Appendix, cf., Eqns. (A.1)-(A.13)). Then the boundary of the plastic zone is determined, and stress components and pressure σ_n on the die are calculated. For the numerical calculations the defining differential equations (8), (23)-(26) are represented in recursive form (A.1)-(A.5). For the initial approximate solution the function $\delta_\theta(r, z)$, which appears in the additional condition (10), is represented in a linear form (A.8) for

neighboring node points of the plastic zone. The dependence (A.8) follows from the first Hencky theorem for the theory of plane deformation of rigid-plastic solids (Hill, 1950).

Eqns. (A.2) and (A.3) are written in view of the sign functions for press forging: $\text{sign}(\sigma_\theta - \sigma_\alpha) = 1$, $\text{sign}(\sigma_\beta - \sigma_\theta) = -1$. The values of the sign functions follow from the representation of possible stress states at press forging by means of Mohr's circle (*cf.*, Figure 6).

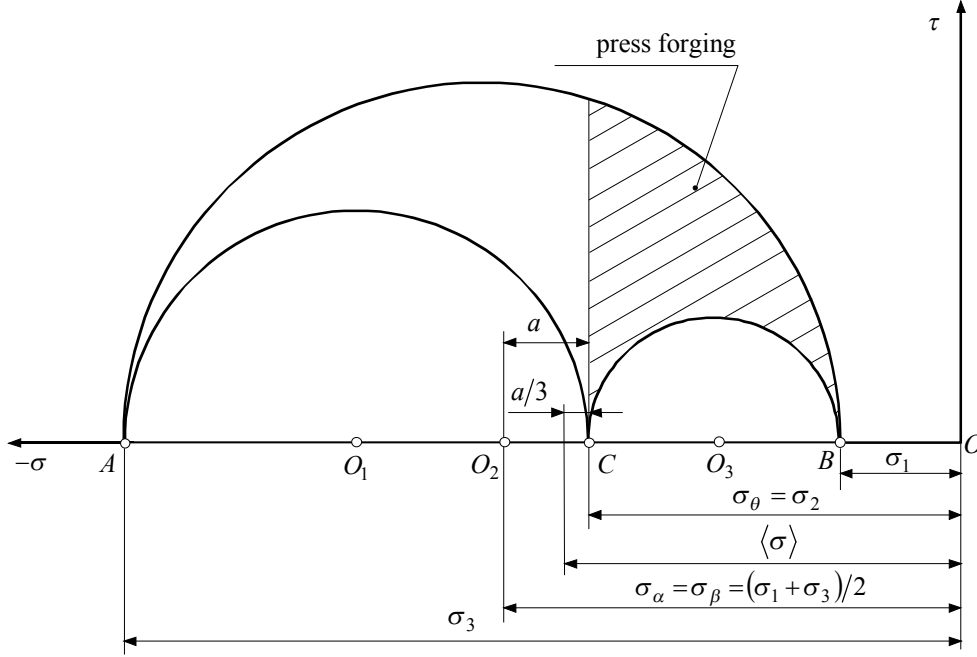


Figure 6. Mohr's circle for the processes of press forging

In fact, possible stress states during press forging are presented for the values of hoop stress $\sigma_\theta = \sigma_2 \in ((\sigma_1 + \sigma_3)/2; \sigma_1]$. The upper limit value $\sigma_\theta = \sigma_1$ corresponds to uniaxial compression and is fulfilled at the symmetry axis of the blank (at $r = 0$). The lower limit value $\sigma_\theta = (\sigma_1 + \sigma_3)/2$ corresponds to pure shear. The stress state close to pure shear (at $\sigma_\theta = 0.85 - 0.90(\sigma_1 + \sigma_3)/2$) is realized in a zone of the material outflow into the radial clearance. Hence, for all combinations of the stress state, we may write $\sigma_\alpha = \sigma_\beta = (\sigma_1 + \sigma_3)/2 < \sigma_\theta$ which confirms previously determined values of the sign functions.

The stress fields in the plastic area of the strained product are defined in each approximation on the basis of a solution of the boundary problems, *e.g.*, after the first stage ($\Delta h_1 = 0.6$ mm, *cf.*, Figure 7, top) the sequence is as follows: degenerate Riemann problem in the zone $A - E - 4.1$, mixed Cauchy problem in the zones $E - 4.1 - 4.4$, $F - 4.4 - 6.4$, $4.4 - 6.4 - 6.6$, $6.4 - 6.5 - C$, Riemann problem in the zone $6.5 - 6.6 - 7.6 - C$ and mixed Cauchy problem in the zone $6.6 - 7.6 - D$. Note that the numbers $m.n$ refer to the indices m and n of the node points which are formed by intersection of the slip lines α_m and β_n (*cf.*, Figure 7, top). It is necessary to mention that the point A on the contact surface of the top die is a singular point of the slip line field (*cf.*, *e.g.*, Kachanov, 2004). This point coincides with the initial slip line β_0 (with the vanished radius of curvature, $R_{\beta_0} \rightarrow 0$) which is contracted to the point. Values of the parametric angle δ_θ in the point A are over the range $[\delta_{\theta 1.0}; \delta_{\theta 4.0}]$ as the slip lines $\alpha_1, \alpha_2, \alpha_3, \alpha_4$ converge to the point A . Hence the node points 1.0, 2.0, 3.0, 4.0 coincide with the point A .

The determined field of the slip lines α and β allow us to define the boundary $AFCDE$ of the plastic area in the meridian cross-section of the half-finished part (Figure 7 shows 1/4 of the meridian cross-section as the plastic area is mirrored w.r.t. the axes of symmetry). When solving these boundary problems we use a condition of maximum contact friction at the end surface of the tool, *i.e.*, $\tau_c = \tau_{\max}$ (τ_{\max} denotes the shearing stress at the contact, index c is for contact). This condition is based on the experimental data showing that high hydrostatic

pressure $\langle \sigma \rangle$ in the die cavity leads to maximum tangential stresses τ_{\max} acting along the contact surface (Unkov *et al.*, 1992).

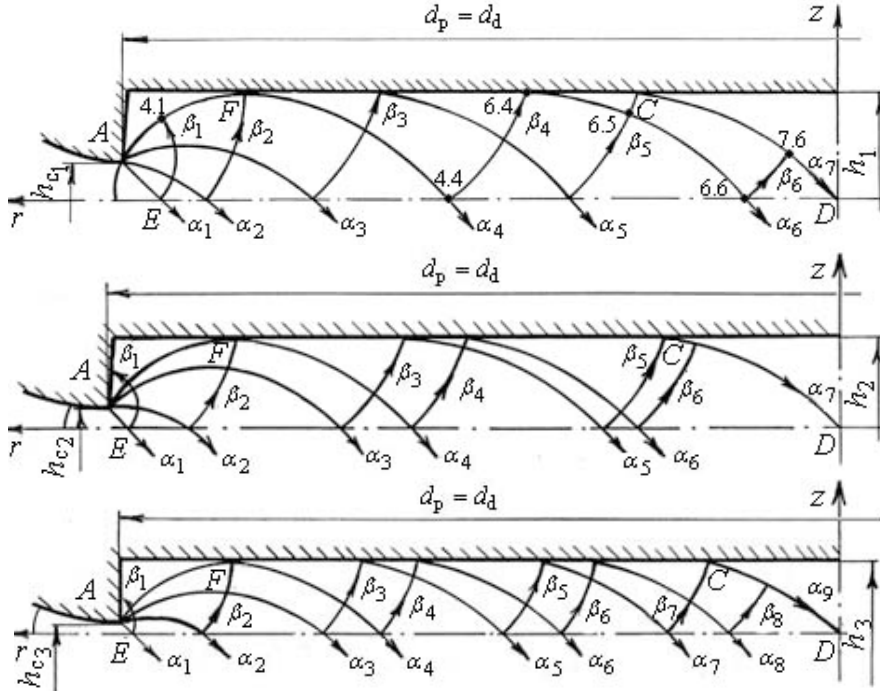


Figure 7. Press forging of an axisymmetric part: the plastic area and the stress field for various displacements of the top die: *top* – $\Delta h_1 = 0.6$ mm, *center* – $\Delta h_2 = 2.5$ mm; *bottom* – $\Delta h_3 = 5.5$ mm

To calculate the average stress $\langle \sigma \rangle$ it is necessary, at first, to find its value in one node point of the plastic area. For this purpose, we use a condition of equilibrium of the material outflowing into a radial clearance

$$\int_{AE} (\sigma_{\alpha} \sin \delta_{\theta} + \tau_{\alpha\beta} \cos \delta_{\theta}) r ds = 0. \quad (32)$$

A numerical solution of the integral equation (32) allows us to find the average stress in the point *A* (*cf.*, Figure 7) (for example, $\sigma_A = -155$ MPa at the final moment of press forging).

For the purpose of a computing procedure it is necessary to note that partial derivatives of a yield stress w.r.t. the coordinates $(\partial \tau_y / \partial s_{\alpha}, \partial \tau_y / \partial s_{\beta})$ that appear in the differential equations (23) and (24). The corresponding re-

cursive equations (A2) and (A3) include relations $\frac{\tau_{y_{m,n+1}} - \tau_{y_{m,n-1}}}{s_{\alpha_{m,n+1}} - s_{\alpha_{m,n-1}}}$ and $\frac{\tau_{y_{m,n+1}} - \tau_{y_{m,n-1}}}{s_{\alpha_{m,n+1}} - s_{\alpha_{m,n-1}}}$. Derivatives (and quanti-

ties in the recursive equations corresponding to them) consider a change of the yield stress in the meridian cross-sections of the deformed material. This change is connected with strain hardening. The strain can be determined in three ways, first, analytically, *e.g.*, using a geometrical theory of deformation (*cf.*, Kachanov, 2004), second, experimentally by coordinate grids (Thomson *et al.*, 1968), and, third, found from known solutions for analogous processes. When calculating the derivatives $\partial \tau_y / \partial s_{\alpha}, \partial \tau_y / \partial s_{\beta}$ the authors use the known solutions for the strain distribution in analogous processes of press forging (Thomson *et al.*, 1968). More accurate distribution of strains can be found from the flow velocity fields determined for different moments of press forging. The exact strain distribution is used when solving the kinetic equations for damage measures.

The material pressure distributed on the contact surface of the top die is $\sigma_n = \sigma_{\beta/z=h}$, where $\sigma_{\beta/z=h}$ is a normal stress in the contact layer of the processed material (at $z = h$) directed along the slip lines β which approach the contact surface at the angle of 90° (*cf.*, Figure 7). The processing force of press forging is

$P = 2\pi \int_0^{d/2} \sigma_n r dr$. The average pressure on the die is $p = P/F_d$, where $F_d = \pi d^2/4$ is the active area of the top die which transfers processing force. The values of $\sigma_{n\max}$, P , and p calculated for the different stages of press forging (Table 2) and the contact pressure (σ_n) diagrams (cf., Figure 8) show their strong change during the process.

Table 2. Force parameters of press forging

Force parameters	Displacements of the top die		
	$\Delta h_1 = 0.60$ mm	$\Delta h_2 = 2.50$ mm	$\Delta h_3 = 5.50$ mm
Maximum pressure on the die, $\sigma_{n\max}$, MPa	1018	1310	1950
Processing force, P , MN	10.8	13.3	15.7
Pressure of press forging, p , MPa	724	890	1050

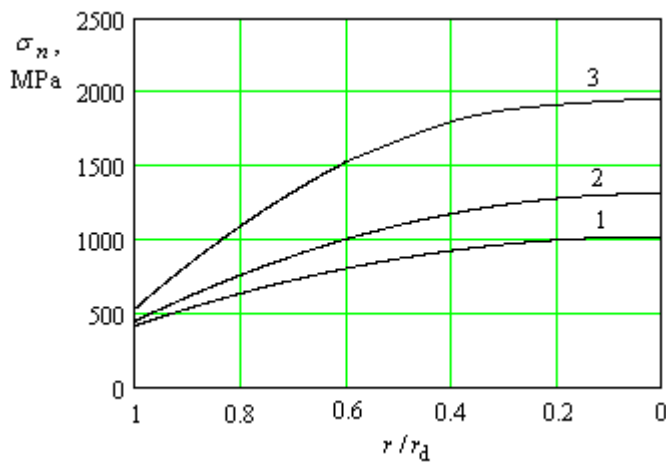
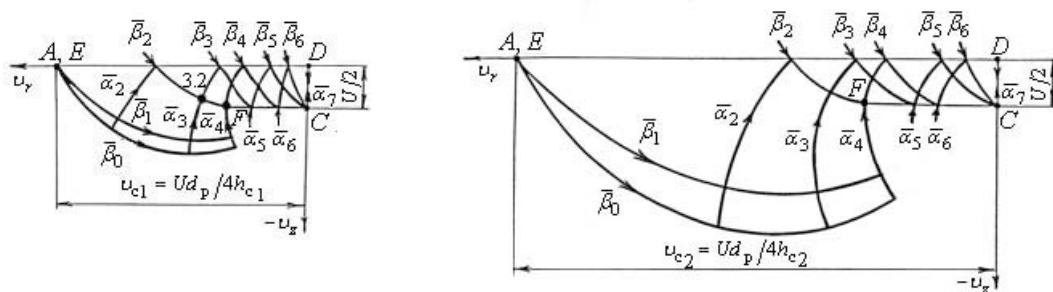


Figure 8. Contact pressure σ_n vs. $\bar{r} = r/r_d$ for various displacements of the top die:
 1 – $\Delta h_1 = 0.6$ mm ; 2 – $\Delta h_2 = 2.5$ mm ; 3 – $\Delta h_3 = 5.5$ mm

The determined fields of slip lines (*i.e.*, the maximum shear stress trajectories $\tau_{\alpha\beta}$) allow us to calculate the fields of plastic flow velocities (*cf.*, Figure 9) by using Eqs. (A.4) and (A.5).



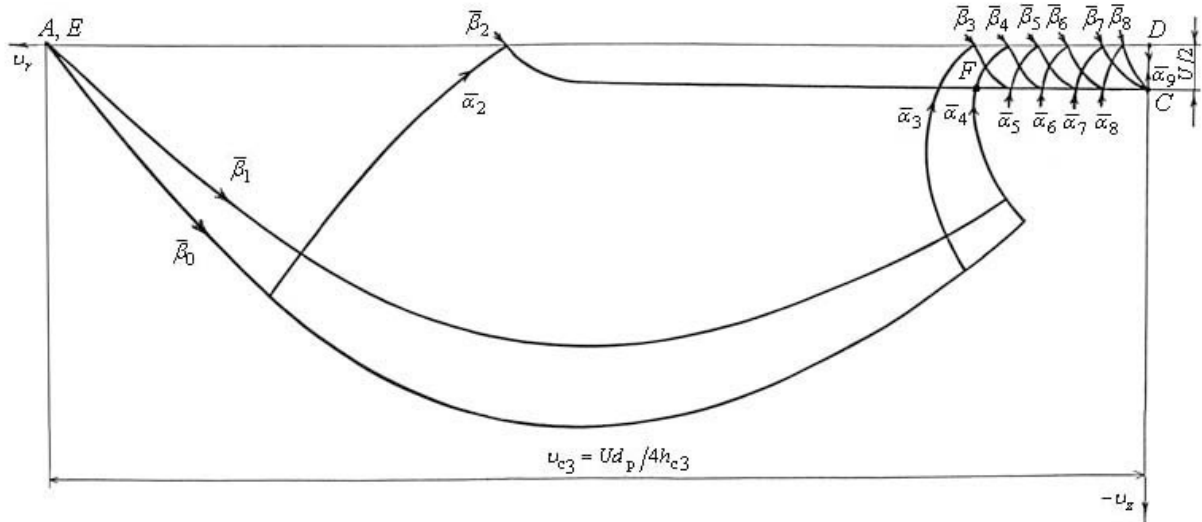


Figure 9. Flow velocity fields for various displacements of the top die:
top left – $\Delta h_1=0.6$ mm , *top right* – $\Delta h_2=2.5$ mm ; *bottom* – $\Delta h_3=5.5$ mm

The parametric angle δ_θ and the trajectory arcs s_α , s_β appearing in Eqs. (A.4) and (A.5) are known from the slip line fields. The field of plastic flow velocities represents a grid of the material lines $\bar{\alpha}$ and $\bar{\beta}$ which coincide with the slip lines α and β in the coordinate system v_r, v_z . Such a representation allows us to find the velocity vector $\bar{v}_{m,n}$ and its components ($v_{r,m,n}, v_{z,m,n}$) for each node point m,n of the plastic area (cf., Figure 10). The radius vector of the represented point m,n is the velocity vector $\bar{v}_{m,n}$ and its components are the velocity components $v_{r,m,n}$ and $v_{z,m,n}$. Thus, representation $\bar{\alpha}, \bar{\beta}$ allows us to determine a dependence of plastic flow velocities on the coordinates of node points, i.e., $v_r(x_{m,n}, y_{m,n})$ and $v_z(x_{m,n}, y_{m,n})$.

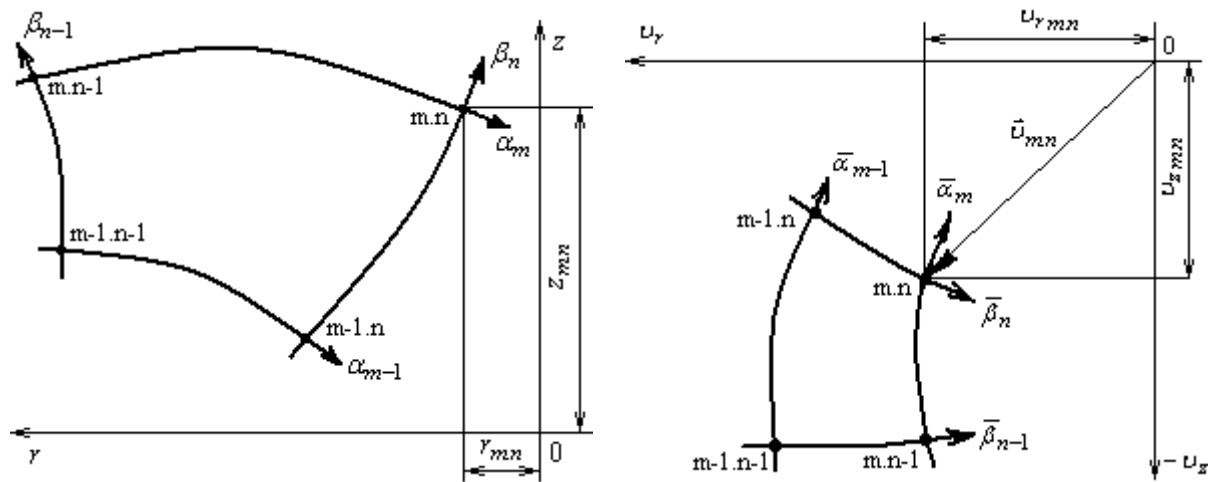


Figure 10. Determination of the material velocity in the node points of the slip line field α, β using representation $\bar{\alpha}, \bar{\beta}$ in the coordinate system v_r, v_z

The following boundary conditions were used when solving the boundary problems (in velocities):
 $v_{\alpha^*} = -U \sin \delta_\theta$, $v_{\beta^*} = -U \cos \delta_\theta$ (along the boundary $AFCD$), $v_{\alpha^*} = -\frac{Ud}{4h_c} \cos \delta_\theta$, $v_{\beta^*} = -\frac{Ud}{4h_c} \sin \delta_\theta$ (along the boundary AE), $v_{\alpha^*} = -v_{\beta^*} = U\sqrt{2}$ (along the line ED), where U is a velocity of the top die movement. The flow velocity fields can be determined by a solution of the boundary problems, e.g., after the first stage ($\Delta h_1=0.6$ mm, cf., Figure 9, *top left*) the sequence is as follows: mixed Cauchy problem in the zone

6.6–7.6–D, Riemann problem in the zone 6.5–6.6–7.6–C, mixed Cauchy problem in the zones 6.4–6.5–C, 4.4–6.4–6.6, F–4.4–6.4, E–4.1–4.4, and Riemann problem in the zone A–E–4.1–4.0. Note that the abbreviation $m.n$ refers to the indices m and n of the node points which are formed by intersection of the lines $\bar{\alpha}_m$ and $\bar{\beta}_n$ mapped onto the meridian plane of velocities v_r, v_z (cf., Figure 9, top left). The boundary points A, F, C, D, E represent the same points of the plastic area. The velocity $v_z = U/2$ is mapped onto the represented fields of plastic flow velocities (cf., Figure 9). This technique simulates a situation when the top die and the counter die move with the equal velocity $U/2$. Such a technique allows us to mirror the fields of velocities w.r.t. the horizontal axis of symmetry and does not affect any results of the subsequent calculations.

The field of velocities should satisfy a kinematic condition according to which a velocity of outflow into the clearance is

$$v_c = -v_{\alpha*} \cos \delta_\theta - v_{\beta*} \sin \delta_\theta = \frac{Ud}{4h_c}. \quad (33)$$

Comparison of velocity diagrams shows that the velocity of outflow into a radial clearance strongly increases during press forging: $v_{c2}/v_{c1} = 1.4$, $v_{c3}/v_{c1} = 2.3$. It should be noted that the field of plastic flow velocities does not contain discontinuities which cross the symmetry axis z , i.e., the velocities of the processed material change continuously during its movement along the trajectories.

A grid of lines $\bar{\alpha}$, $\bar{\beta}$ selected in the plastic zone consists of continuum points. This grid is coincident with a grid of slip lines α , β at the observed moment of deformation. This grid of the material lines of continuum, $\bar{\alpha}$, $\bar{\beta}$, can be considered as associated coordinate frame (Sedov, 1983), and plotted velocity fields (cf., Figure 9) can be considered as a representation of the material lines $\bar{\alpha}$, $\bar{\beta}$ in the velocity plane. A similar representation of the flow velocity field is essential for the following kinematic analysis of the non-stationary processes.

The flow velocity field has the following features at axisymmetric press forging (cf., Figure 9): The mutual orthogonality of the lines $\bar{\alpha}$ and $\bar{\beta}$ is virtually kept when we map the lines $\bar{\alpha}$, $\bar{\beta}$, which are close to the radial clearance of the die (lines $\alpha_1, \alpha_2, \beta_1, \beta_2$), onto the plane of velocities v_r, v_z . This is typical for pure shear (plane deformation) in this area of the deformed metal. The angle between the tangents of continuum lines $\bar{\alpha}$ and $\bar{\beta}$ increasingly changes in their intersection points when we map the lines $\bar{\alpha}$ and $\bar{\beta}$ onto the plane of velocities v_r, v_z . Finally, when we map the node points which are located at the symmetry axis, the level lines of the velocity vector v_z converges in the range from 0 to v_d . For these points the mapped angle between the continuum lines $\bar{\alpha}$ and $\bar{\beta}$ is equal to $\pi/2$ (the lines α and β are mapped in opposite phase) which is typical for uniaxial states. Thus, a representation of the continuum lines $\bar{\alpha}$ and $\bar{\beta}$ in the plane of velocities v_r, v_z is dependent on the Lode angles $\phi_\sigma, \phi_\epsilon$ of the stress (s_{ij}) and the strain rate ($\dot{\epsilon}_{ij}$) deviators, respectively.

The degree of conformity between the fields of stresses $\sigma_{ij}^{(0)}$ and velocities $v_i^{(0)}$ in the initial approximate solution is determined by fulfilling the similarity condition (4) for deviators $\dot{\epsilon}_{ij}$ and s_{ij} in the form:

$$m_\theta^{(\dot{\epsilon})} - m_\theta^{(\sigma)} \leq [\Delta m_\theta], \quad (34)$$

$[\Delta m_\theta]$ being a permissible mismatch error for the parameters $m_\theta^{(\dot{\epsilon})}$ and $m_\theta^{(\sigma)}$ related to the fields of stresses and strain rates (cf., Eqn. (A.13) and Figure A.1).

For the solution of the inequality (34) the method of group relaxation is used (e.g., Korn and Korn, 2000, Section 20.3-2). By regulating the absolute value of the difference between the parameters $m_\theta^{(\dot{\epsilon})}$ and $m_\theta^{(\sigma)}$ in selected nodes of the plastic zone (instead of its complete liquidation at the first step) it is possible to fulfill the inequality

(34) already at the first correction with the permissible error $[\Delta m_\theta] = 0.01$. The calculated stress field (*cf.*, Figure 7) and the corresponding field of flow velocities (*cf.*, Figure 9) satisfy the inequality (34) for the permissible error $[\Delta m_\theta] = 0.01$.

4.2 Determination of cumulative strains

The cumulative strain Λ and its rate $\dot{\Lambda}$ appears in the kinetic equations (7) for the meso-structural parameters μ_k by means of the parameter χ_s . Λ and $\dot{\Lambda}$ also appear in Eqn. (27) for the damage measure ω_1 which is connected to the plastic dilatation of the deformed material due to the volume growth of the voids. The consistent fields of stresses (σ_{ij}) and plastic flow velocities (v_i) found at different stages of non-stationary deformation allow us to calculate strain rates $\dot{\Lambda}$, strain increments $\Delta\Lambda$, and cumulative strains Λ along the trajectories of the movement of the material particles. The trajectories for particles of the deformed material can be described in terms of the coordinates α^* , β^* , t by the following differential equations:

$$\frac{ds_{\alpha^*}}{dt} = v_{\alpha^*}(\alpha^*, \beta^*, t), \quad \frac{ds_{\beta^*}}{dt} = v_{\beta^*}(\alpha^*, \beta^*, t). \quad (35)$$

The fields of slip lines and flow velocities allow us to integrate Eqns. (35) numerically (*i.e.*, step-by-step): $\Delta s_{\alpha^*} = v_{\alpha^*} \Delta t$, $\Delta s_{\beta^*} = v_{\beta^*} \Delta t$, where Δs_{α^*} , Δs_{β^*} are projections of the vector $\Delta \vec{s}$, which defines a directed increment of the trajectory at the current stage, Δt being the time of the current loading stage. For the press forging process the time t is substituted for the top die displacement h (time-like parameter of the process), *i.e.* $\Delta t_i = \Delta h_i / v_p$ for the i -th stage of deformation. The trajectories of movement for particles of the deformed material in the plastic area (*cf.*, Figure 11) are found by numerical integration of the differential equations (35). The initial coordinates of the chosen particles G, K, L, M, N, R, S, T are defined at the moment $d/h = 7.1$ by intersection of the surfaces $r = -0.125d$, $r = -0.25d$, $r = -0.375d$, $r = -0.475d$, and the planes $z = 0.25h$ and $z = 0.5h$. Figure 11 shows trajectories of the material particles for 1/4 of a meridian cross-section of the billet (to the left and above the axes of symmetry). Trajectories of the rest part of the meridian cross-section are mirrored w.r.t. the axes of symmetry.

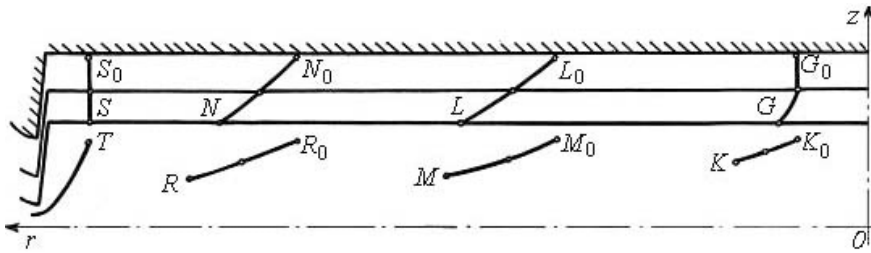


Figure 11. Trajectories of particles of the deformed material (in the layer with the Lagrange coordinate $z = 0.25h_b$) in the radial direction r at the final moment of press forging

Now we will determine the strain cumulated by the material particles along the trajectories of their movement. The non-vanishing components of the strain increments in the coordinates α^* , β^* , θ are

$$\begin{aligned} de_\alpha &= \left(\frac{\partial v_{\alpha^*}}{\partial s_\alpha} - v_{\beta^*} \frac{\partial \delta_\theta}{\partial s_\alpha} \right) dt, \quad de_\beta = \left(\frac{\partial v_{\beta^*}}{\partial s_\beta} + v_{\alpha^*} \frac{\partial \delta_\theta}{\partial s_\beta} \right) dt, \quad de_\theta = \frac{v_{\alpha^*} \cos \delta_\theta - v_{\beta^*} \sin \delta_\theta}{r} dt, \\ d\gamma_{\alpha\beta} &= \left(\frac{\partial v_{\alpha^*}}{\partial s_\beta} - v_{\beta^*} \frac{\partial \delta_\theta}{\partial s_\beta} + \frac{\partial v_{\beta^*}}{\partial s_\alpha} + v_{\alpha^*} \frac{\partial \delta_\theta}{\partial s_\alpha} \right) dt, \end{aligned} \quad (36)$$

or according to the rule of differentiation of vector components in a curvilinear coordinate system

$$de_\alpha = \frac{dv_{\alpha^*}}{v_\alpha}, \quad de_\beta = \frac{dv_{\beta^*}}{v_\beta}, \quad de_\theta = -\left(\frac{dv_{\alpha^*}}{v_\alpha} + \frac{dv_{\beta^*}}{v_\beta}\right), \quad d\gamma_{\alpha\beta} = \frac{dv_{\alpha^*}}{v_\beta} + \frac{dv_{\beta^*}}{v_\alpha}, \quad (37)$$

where v_α and v_β are the flow velocity components relative to a moving grid of the characteristics (differential equations of equilibrium (25) and (26) and differential equations of velocities (25) and (26) are both of hyperbolic type and have two sets of characteristics α and β coinciding with the slip lines).

In view of the obvious relations $de_\alpha = de_\beta$ and $de_\theta = -2de_\alpha = -2de_\beta$ we may obtain the following dependence for the intensity of the shear strain increment ($d\Lambda$)

$$d\Lambda = \sqrt{12(de_\alpha)^2 + (d\gamma_{\alpha\beta})^2} = \sqrt{3\left(\frac{dv_{\alpha^*}}{v_\alpha} + \frac{dv_{\beta^*}}{v_\beta}\right)^2 + \left(\frac{dv_{\alpha^*}}{v_\beta} + \frac{dv_{\beta^*}}{v_\alpha}\right)^2}, \quad (38)$$

or for a short stage k of deformation

$$\Delta\Lambda_k = \sqrt{3\left(\frac{\Delta v_{\alpha^*}}{v_\alpha} + \frac{\Delta v_{\beta^*}}{v_\beta}\right)^2 + \left(\frac{\Delta v_{\alpha^*}}{v_\beta} + \frac{\Delta v_{\beta^*}}{v_\alpha}\right)^2},$$

where the components $\Delta v_{\alpha^*} = (v_{\alpha^*})_k - (v_{\alpha^*})_{k-1}$ and $\Delta v_{\beta^*} = (v_{\beta^*})_k - (v_{\beta^*})_{k-1}$ can be found by the fields of plastic flow velocities.

The components v_α , v_β relative to a moving grid of the characteristics α , β at non-stationary flow are

$$v_\alpha = v_{\alpha^*} - v_{\alpha^*}^*, \quad v_\beta = v_{\beta^*} - v_{\beta^*}^*, \quad (39)$$

$v_{\alpha^*}^*$, $v_{\beta^*}^*$ denoting the velocity components of a moving grid of the characteristics α , β .

When considering a grid of the characteristics α , β as the intersection of two sets of mutually orthogonal surfaces $\omega_\alpha(r, z, t) = 0$ and $\omega_\beta(r, z, t) = 0$ by the planes $t = \text{const}$ (in the space r, z, t) it is possible to use the following equations in terms of complete differentials

$$\frac{\partial\omega_\alpha}{\partial s_\alpha} ds_\alpha + \frac{\partial\omega_\alpha}{\partial s_\beta} ds_\beta + \frac{\partial\omega_\alpha}{\partial t} dt = 0, \quad \frac{\partial\omega_\beta}{\partial s_\alpha} ds_\alpha + \frac{\partial\omega_\beta}{\partial s_\beta} ds_\beta + \frac{\partial\omega_\beta}{\partial t} dt = 0. \quad (40)$$

It is obvious that the derivatives $\partial\omega_\alpha/\partial s_\alpha$, $\partial\omega_\beta/\partial s_\beta$ vanish since the surfaces $\omega_\alpha = 0$ and $\omega_\beta = 0$ are characteristics. By virtue of Eqns. (39) we may find the velocity components for a grid of the characteristics α , β :

$$v_{\alpha^*}^* = -\frac{\partial\omega_\beta/\partial t}{\partial\omega_\beta/\partial s_\alpha}, \quad v_{\beta^*}^* = -\frac{\partial\omega_\alpha/\partial t}{\partial\omega_\alpha/\partial s_\beta}, \quad (41)$$

and the following relations for its kinematic properties

$$\frac{\partial v_{\alpha^*}^*}{\partial s_\beta} - v_{\beta^*}^* \frac{\partial \delta_\theta}{\partial s_\beta} = 0, \quad \frac{\partial v_{\beta^*}^*}{\partial s_\alpha} - v_{\alpha^*}^* \frac{\partial \delta_\theta}{\partial s_\alpha} = 0. \quad (42)$$

If a moving grid of the characteristics α , β is considered as the material continuum then its strain rate components are

$$\dot{e}_\alpha^* = \frac{\partial v_{\alpha^*}^*}{\partial s_\alpha} - v_{\beta^*}^* \frac{\partial \delta_\theta}{\partial s_\alpha}, \quad \dot{e}_\beta^* = \frac{\partial v_{\beta^*}^*}{\partial s_\beta} - v_{\alpha^*}^* \frac{\partial \delta_\theta}{\partial s_\beta}, \quad \gamma_{\alpha\beta}^* = \frac{\partial v_{\alpha^*}^*}{\partial s_\beta} - v_{\beta^*}^* \frac{\partial \delta_\theta}{\partial s_\beta} + \frac{\partial v_{\beta^*}^*}{\partial s_\alpha} - v_{\alpha^*}^* \frac{\partial \delta_\theta}{\partial s_\alpha} = 0, \quad (43)$$

i.e., a grid of the characteristics is subject to an extension or a compression, but not to shear during its translational movement *w.r.t.* a fixed reference frame α^*, β^* . This means that the parametric angle δ_θ varies over $\pm\pi$ when a grid of the characteristics α, β is mapped onto velocity plane. Thus, the kinematic relations (42) represented in the recursive form (A.6) and (A.7) allow us to map fields of the characteristics α, β onto the velocity plane (*cf.*, Figure 12). This mapping allows us to find the velocity vector $\vec{v}_{m.n}^*$ and its components $v_{r.m.n}^*, v_{z.m.n}^*$ (or $v_{\alpha^* m.n}^*, v_{\beta^* m.n}^*$ in the coordinates α^*, β^*) for each node point $m.n$ of the moving grid of the characteristics (by analogy with determination of the material velocity in the node points of the slip line field α, β by means of representation $\bar{\alpha}, \bar{\beta}$ in the coordinates v_r, v_z , *cf.*, Figure 10) and to calculate the velocity components v_α, v_β by the dependences (42) at each stage k

$$(v_\alpha)_k = \frac{1}{2} [(v_{\alpha^*})_{k-1} + (v_{\alpha^*})_k - (v_{\alpha^*})_{k-1} - (v_{\alpha^*})_k], \quad (44)$$

$$(v_\beta)_k = \frac{1}{2} [(v_{\beta^*})_{k-1} + (v_{\beta^*})_k - (v_{\beta^*})_{k-1} - (v_{\beta^*})_k].$$

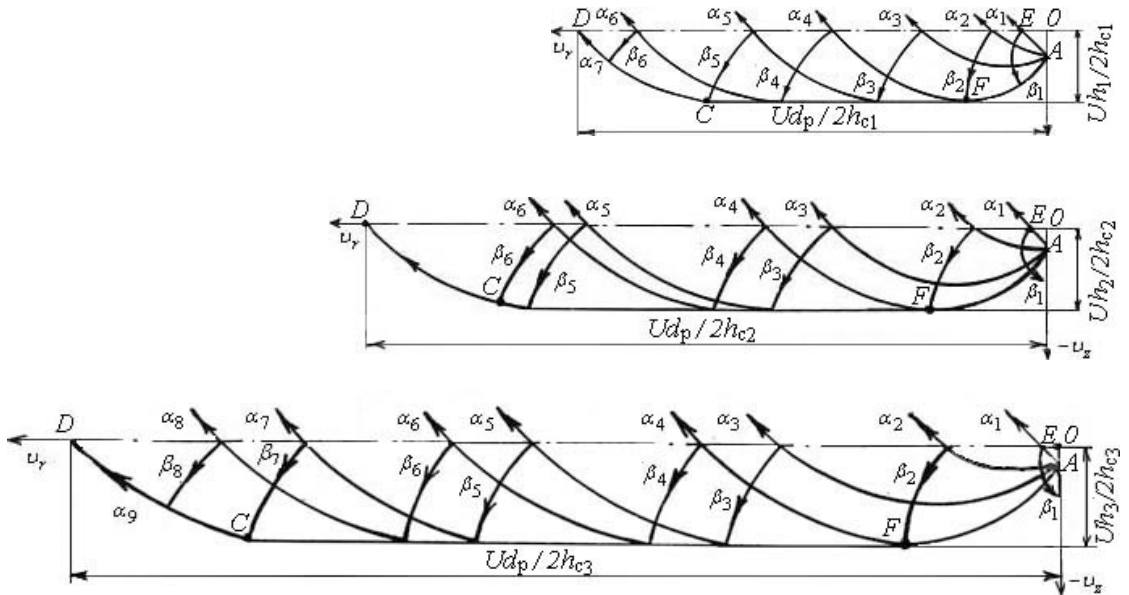


Figure 12. The fields of velocities v_α^*, v_β^* of characteristics for various displacements of the top die: *top* – $\Delta h_1 = 0.6$ mm, *center* – $\Delta h_2 = 2.5$ mm; *bottom* – $\Delta h_3 = 5.5$ mm

The cumulative strains after stage k are $\Lambda_k = \sum_{j=1}^k \Delta\Lambda_j$, and $\Lambda = \sum_{j=1}^n \Delta\Lambda_j$ at the end of forming. In Figure 13 the distribution of the cumulative strains Λ is shown for the layer with the Lagrange coordinate $z = 0.25h_b$ in the radial direction r at the final moment of press forging. The diagram for $\Lambda(r)$ shows that the most intense strain is experienced by the metal particles that intersect a boundary of the plastic area or come close to it at the final moment of press forging. Large finite strains in the zone with outflow into the radial clearance result in intensive thermal flux and heating of the processed metal up to 350°C and higher. According to the rheological dependence (29), a distribution of the strain Λ allows us to refine a distribution of the mechanical properties of the processed material, *i.e.*, the yield stress in node points of the slip line field. Figure 13 (*left*) shows a distribution of the yield stress σ_y in the radial direction r of the layer with the Lagrange coordinate $z = 0.25h_0$. The slip lines fields (*i.e.*, the stresses σ_{ij}) together with a refined distribution of the yield stress σ_y (or equivalent stress

$s = \tau_y = \sigma_y / \sqrt{3}$) allow us to determine the stress triaxiality $\langle \bar{\sigma} \rangle = \langle \sigma \rangle / s = \langle \sigma \rangle / \tau_y$ in node points of the plastic area at the considered moments of press forging (*cf.*, Figure 13).

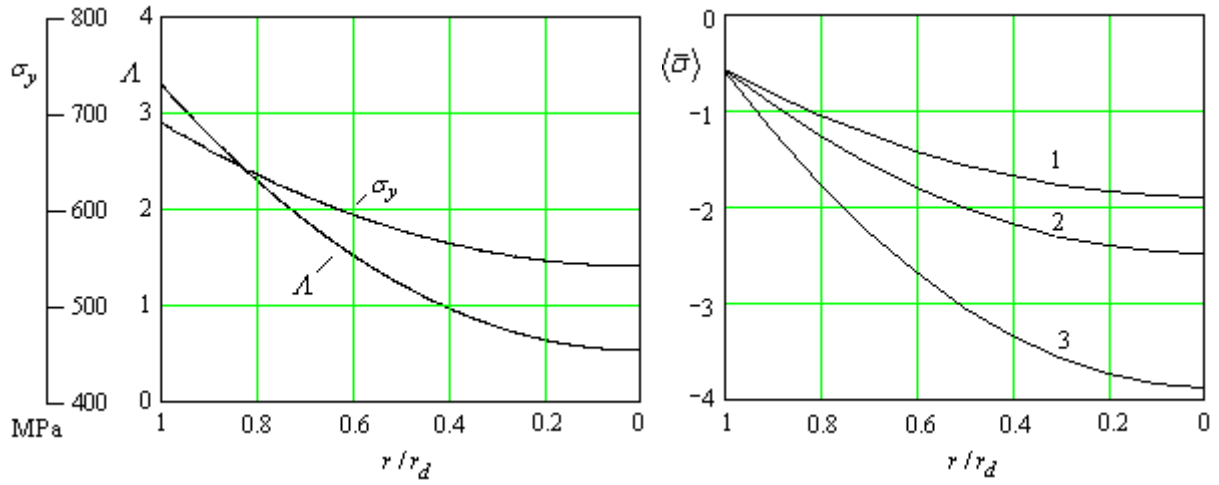


Figure 13. Distribution of the parameters Λ and σ_y at the final moment of press forging (*left*) and triaxiality $\langle \bar{\sigma} \rangle$ for various displacements of the top die (*right*): 1 – $\Delta h_1 = 0.6$ mm , 2 – $\Delta h_2 = 2.5$ mm ; 3 – $\Delta h_3 = 5.5$ mm , in the layer with the Lagrange coordinate $z = 0.25 h_b$ in the radial direction

4.3 Determination of strain damage

The strain damage of the finished part can be predicted by numerical integration of Eqns. (27) and (28) for the damage parameters ω_1 and ω_2 . The function of plastic dilatation, $\varepsilon_i^i(\Lambda)$, that appears in Eqn. (27), is of the power type, $\varepsilon_i^i(\Lambda) = b\Lambda^a$, where b and a denote experimentally determined parameters (*cf.*, Table 3). Therefore Eqn. (27) becomes

$$d\omega_1 = \frac{a\Lambda^{a-1}}{\Lambda_{\text{lim}}^a} d\Lambda . \quad (45)$$

The limit cumulative strain at shear, Λ_{lim} , appearing in Eqn. (45), corresponds to the destruction of the deformed material. The limit strain Λ_{lim} is determined by experimental diagrams of plasticity plotted for the investigated steel under prescribed temperature-speed conditions (*cf.*, Figure 14). Plasticity diagrams represent the experimentally determined dependence of the limit strain Λ_{lim} on stress triaxiality $\langle \bar{\sigma} \rangle$, which can be approximated by a power function in the following form

$$\Lambda_{\text{lim}} = A \cdot \exp(-\langle \bar{\sigma} \rangle) + B \cdot \exp(-c\langle \bar{\sigma} \rangle), \quad (46)$$

where A, B, c are the experimentally determined parameters (*cf.*, Table 3).

Proceeding in Eq. (45) with small finite increments of the strain ($\Delta\Lambda$) we may find the material damage after the k -th stage of deformation by numerical integration

$$\omega_{1k} = \omega_{10} + \sum_{j=1}^k \Delta\omega_{1j}, \quad \Delta\omega_{1j} = \frac{a\Lambda_j^{a-1}}{\Lambda_{\text{lim}}^a(\langle \bar{\sigma} \rangle_j)} \Delta\Lambda_j, \quad (47)$$

where ω_{10} is the damage of the as-delivered material (*cf.*, Table 3), Λ_j is the strain accumulated by the material particles up to the j -th stage, $\Lambda_{\text{lim}}(\langle\bar{\sigma}\rangle_j)$ is the limit strain corresponding to stress triaxiality $\langle\bar{\sigma}\rangle_j$ at the j -th stage. Calculations of the damage measure ω_2 by means of numerical integration of the kinetic equation (28) are connected to the determination of the equivalent deviatoric strain rate of voids $\dot{\bar{e}}$, and the critical deviatoric strain \bar{e}_{cr} corresponding to a stage of intense coalescence of ellipsoidal voids and formation of cavernous defects. Calculations of the equivalent strain rate of voids necessitate an experimental determination of their dimensions changing under deformation (Chen *et al.*, 2002; Lemaitre and Desmorat, 2007; Voyiadjis and Kattan, 2006). The determination of the critical equivalent strain \bar{e}_{cr} of voids in the investigated materials is based on microscopic analysis of void coalescence in test specimens during their stage-by-stage plastic deformation. The obtained micrographs will allow us to detect a stage of intense void coalescence into large cavernous defects. Such experiments involve great technical difficulties (Krajcinovic, 2000). This is why we shall make use of statistical characteristics of void formation.

For instance, an average equivalent strain rate can be applied within each Representative Volume Element (RVE). A corresponding measure is the equivalent strain rate (\dot{e}) of the RVE. The hypothesis that it is possible to model the void deformation by using the strain measures of the RVE requires detailed experimental verification. The experimental justification of this hypothesis will allow us to predict shape changes and coalescence of voids by means of accompanying axes ξ^i plotted as coordinate grids on deformed specimens and manufacturing blanks. The hypothesis allows us to accept in our case $\dot{\bar{e}}(r, z, t) = \dot{e}(r, z, t)$, where the function $\dot{e}(r, z, t)$ can be established by a distribution of the equivalent strain increments $\Delta e(r, z, h)$ in cells of the coordinate grid, *i.e.*, $\dot{e}(r, z, t) \cong \Delta e(r, z, t) / \Delta t = v_p \cdot \Delta e(r, z, h) / \Delta h$.

In order to find the critical equivalent strain of voids, \bar{e}_{cr} , the experimental results obtained by Bogatov *et al.* (1984) were used. They investigated void coalescence and formation of cavernous defects in some structural metals at forming. Electron-probe analysis of the micro-structure of stepwise deformed metals allowed them to verify that the critical equivalent strain of voids can be expressed as $\bar{e}_{cr} = 0.6 \cdot e_{\text{lim}} \exp[0.05(1 - \langle\bar{\sigma}\rangle)]$, where $e_{\text{lim}} = \Lambda_{\text{lim}}/2$ is the limit deviatoric strain of RVE corresponding to the moment of its destruction. In view of the given experimental data Eq. (28) becomes

$$d\omega_2 = \frac{5 \cdot \exp[0.05(\langle\bar{\sigma}\rangle - 1)]}{3 \cdot e_{\text{lim}}} de. \quad (48)$$

By using small finite strain increments, Δe , in Eq. (48) we may calculate the material damage ω_2 after the k -th stage of deformation by numerical integration

$$\omega_{2k} = \omega_{20} + \sum_{j=1}^k \Delta\omega_{2j}, \quad \Delta\omega_{2j} = \frac{5 \cdot \exp[0.05(\langle\bar{\sigma}\rangle_j - 1)]}{3 \cdot e_{\text{lim}j}} (\Delta e)_j, \quad (49)$$

where ω_{20} is the damage of the as-delivered material (*cf.*, Table 3), and $e_{\text{lim}j}$ is the limit deviatoric strain corresponding to the stress state parameter $\langle\bar{\sigma}\rangle_j$ at the j -th stage of deformation.

Table 3. Material parameters for calculations of damage

C in steel, %	Parameters of plastic dilatation		Parameters of limit plasticity			Damage of the as-delivered material	
	b	a	A	B	c	ω_{10}	ω_{20}
0.08-0.10	0.032	1.193	-0.222	2.042	0.560	0-0.10	0-0.12
0.18-0.20	0.033	1.263	-0.156	1.656	0.550	0-0.10	0-0.12

The cumulative strain Λ (including the equivalent strain $e = \Lambda/\sqrt{3}$) and stress triaxiality $\langle\bar{\sigma}\rangle$ appears in the constitutive equations for damage measures (27), (45), (46), (48). We have the complete information which is required to calculate damage measures by means of Eqs. (47) and (49). Moreover, we know the mechanical and meso-structural parameters of the steel (*cf.*, Tables 1 and 3) as well as stepwise values of the strain, $\Delta\Lambda_i$, and the limit strain Λ_{lim} (as the known function of stress triaxiality $\langle\bar{\sigma}\rangle$, *cf.*, (46)).

In Figure 14 the predicted distribution of damage (ω_1 and ω_2) is shown for the radially directed middle layer of the finished product (with the coordinate $z=0.25h_0$). The observed fact that the damage increases from the symmetry axis towards the flange can be explained as follows. First, the strain (Λ) accumulated by the material particles along their trajectories (which are directed towards the radial clearance of the die) increases in the same direction. Second, large compressive hydrostatic stress $\langle\sigma\rangle$ prevents the evolution of damage, and indeed, the absolute value of $\langle\sigma\rangle$ increases when moving from the radial clearance toward the axis of symmetry.

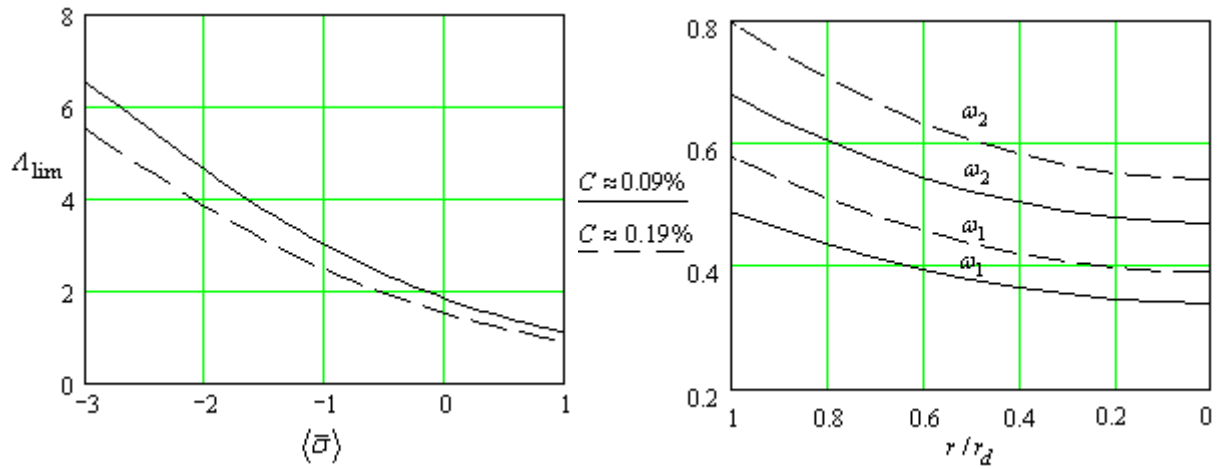


Figure 14. Limit strain Λ_{lim} vs. triaxiality $\langle\bar{\sigma}\rangle$ (*left*) and damage ω_1 and ω_2 vs. relative radius $\bar{r} = r/r_d$ (*right*)

Also note in Figure 14 that the growth rate of ω_2 is higher than that of ω_1 . The ratio of the increments $d\omega_2/d\omega_1 > 1$ follows from Eqs. (45) and (48). For example, $d\omega_2/d\omega_1 = 1.3-1.6$ when the triaxiality is $\langle\bar{\sigma}\rangle = -3-0.67$, which is typical for MF processes. In other words, this ratio is greater for tensile regimes of the stress state ($\langle\bar{\sigma}\rangle > 0$) than for compressive ones ($\langle\bar{\sigma}\rangle < 0$). These relations are physically obvious. Void coalescence always advances macro-crack formation. And during tensile loading regimes (when tensile stresses promote void growth) this advance will be greater than during compressive ones.

The predicted values of damage induced by micro-defects are much less than allowed ones

$$\omega_{1max} = 0.49 - 0.58 < \omega_{1lim} = 1, \quad \omega_{2max} = 0.68 - 0.80 < \omega_{2lim} = 1. \quad (50)$$

where the lower calculated values of damage (0.49 and 0.68) correspond to the steel with carbon content $C: 0.08-0.10\%$ since the upper values (0.58 and 0.80) correspond to $C: 0.18-0.20\%$.

Medium damage of the finished part can be explained, first of all, by high hydrostatic pressure that heals micro-defects in the plastic zone, prevents their growth and, thereby, enhances the processing ductility of the deformed metal. Thus, larger processing strains are possible during press forging (up to 85% and more).

5 Conclusions

The enhanced method of slip lines is used here in order to obtain the rapid and accurate solution of the applied problem of press forging. The results allow us to make the following conclusions: The state of stress of the deformed metal changes substantially throughout its volume, from uniaxial compression at the symmetry axis to pure shear close to compression nearby a radial clearance between the top die and the counter die. This fact is the result of a complex loading of the processed material, *i.e.*, a change in the ratio between the principal stresses and strain rates along the movement trajectories of material particles. A change in the ratio between the principal stresses $\sigma_1, \sigma_2, \sigma_3$ and the principal strain rates $\dot{\epsilon}_1, \dot{\epsilon}_2, \dot{\epsilon}_3$ is defined by a phase angle of the stress deviator s_{ij} and the strain rate deviator $\dot{\epsilon}_{ij}$, *i.e.*, the Lode angles ϕ_σ and ϕ_ϵ , respectively. According to our calculations the Lode angles change from the symmetry axis towards a radial clearance between the top die and the counter die over the range $\phi_\epsilon, \phi_\sigma = 0 - 0.35$. This condition necessitates a determination of consistent fields of stresses and flow velocities in the plastic area taking into account that the condition of similarity between strain rate and stress deviators ($\phi_\epsilon = \phi_\sigma$) should be satisfied in all nodal points.

The similarity condition for the deviators $\dot{\epsilon}_{ij}$ and s_{ij} is identically fulfilled during plane plastic flow when Lode angles correspond to pure shear ($\phi_\epsilon = \phi_\sigma = \pi/6$). When processes with non-stationary axisymmetric flow are analyzed it is very difficult to fulfill the similarity condition ($\phi_\epsilon = \phi_\sigma$) in all nodal points of the plastic area. The reason is a complex numerical procedure of coordinating the stress and the flow velocity fields. The enhanced method of slip lines, based on a representation of yield zones in deviatoric stress space, allows us to implement this numerical procedure.

The cumulative strains are irregularly distributed in the meridian cross-sections of the part. The largest strain is accumulated by the material particles that appear out of the plastic zone or approach to its neighborhood at the final moment of processing. The reliability of the predicted mechanical and mesostructural characteristics depends on the accuracy of the calculated strain field. The strains that were experimentally determined from a coordinate grid satisfactorily agree with the theoretically calculated strains.

Comparison between the maximum values of damage measures and their allowed values, *i.e.*, $\omega_{1\max} = 0.49 - 0.58 < \omega_{1\lim} = 1$, $\omega_{2\max} = 0.68 - 0.80 < \omega_{2\lim} = 1$, allows us to predict the quality of the material structure after press forging. Moderate damage can be explained by the effect of a large compressive hydrostatic stress $\langle \sigma \rangle$ which prevents void growth and coalescence. Large processing strain at press forging provides high strength properties of products due to strain hardening. The carbon content in steels substantially affects the damage induced by strain.

The combined use of two damage measures, ω_1 and ω_2 , in contrast to using only ω_1 or the volume fraction of voids, f_v , as in the known common models (*cf.*, *e.g.*, McClintock, 1968; Rice and Tracey, 1969; Kachanov, 1986; Gurson, 1977), allows us to predict not only a risk of macro-fracture of the deformed material but even the stage of formation of large cavernous defects due to coalescence of voids taking a change in their shape and orientation into account. For example, under large processing deformation it can happen that $\omega_1 < 1$ while $\omega_2 = 1$. *In this case using only one measure (ω_1 or f_v) for calculations would indicate non-criticality of damage while the second measure ($\omega_2 = 1$) reveals a critical stage of voids coalescence and generation of cavities.* This situation is undesirable or even unacceptable when producing metalware to be operated under intense loading and thermal actions which is widespread in aerospace, automotive and energy engineering.

It should be noted that a successful practical application of tensor theory to modeling of MF processes requires rather laborious experimental research on damage kinetics for deformed materials under complex loading. Such experiments will promote the creation of a database for meso-structural properties of plastically deformed materials which is necessary for computer simulations. To this end the authors have already begun their experimental research on the growth, shape change, and coalescence of meso-defects during stepwise plastic deformation of some structural metals.

Appendices

A.1 The recursive form of the basic differential equations for axisymmetric deformation of a plastically rigid solid

For the numerical solution of the basic differential equations (8), (23)-(26) and (42) for axisymmetric deformation of a rigidly-plastic solid the following recursive form can be used

$$z_{m,n} - z_{m,n-1} = (r_{m,n} - r_{m,n-1}) \tan \frac{\delta_{\theta m,n-1} + \delta_{\theta m,n}}{2}, \quad z_{m,n} - z_{m-1,n} = -(r_{m,n} - r_{m-1,n}) \cot \frac{\delta_{\theta m-1,n} + \delta_{\theta m,n}}{2}, \quad (\text{A.1})$$

$$\begin{aligned} & \frac{\sigma_{m,n+1} - \sigma_{m,n-1} - 2\tau_{y m,n} m_{\theta m,n}}{s_{\alpha m,n+1} - s_{\alpha m,n-1}} \left[1 + \sqrt{\frac{2}{3}} \varphi'_{\theta}(\delta_{\theta m,n}) \right] \frac{\delta_{\theta m,n+1} - \delta_{\theta m,n-1}}{s_{\alpha m,n+1} - s_{\alpha m,n-1}} + \\ & + \tau_{y m,n} \frac{m_{\theta m,n}}{\sqrt{3} \sqrt{1 - m_{\theta m,n}^2}} \text{sign}(\sigma_{\theta m,n} - \sigma_{\alpha m,n}) \frac{m_{\theta m,n+1} - m_{\theta m,n-1}}{s_{\alpha m,n+1} - s_{\alpha m,n-1}} - \\ & - \sqrt{3} \frac{\tau_{y m,n}}{r_{m,n}} \sqrt{1 - m_{\theta m,n}^2} \cos \delta_{\theta m,n} \text{sign}(\sigma_{\theta m,n} - \sigma_{\alpha m,n}) - \frac{\sqrt{1 - m_{\theta m,n}^2}}{\sqrt{3}} \text{sign}(\sigma_{\theta m,n} - \sigma_{\alpha m,n}) \frac{\tau_{y m,n+1} - \tau_{y m,n-1}}{s_{\alpha m,n+1} - s_{\alpha m,n-1}} + \\ & + \tau_{y m,n} \frac{m_{\theta m+1,n} - m_{\theta m-1,n}}{s_{\beta m+1,n} - s_{\beta m-1,n}} - \tau_{y m,n} \frac{m_{\theta m,n}}{r_{m,n}} \sin \delta_{\theta m,n} + m_{\theta m,n} \frac{\tau_{y m+1,n} - \tau_{y m-1,n}}{s_{\beta m+1,n} - s_{\beta m-1,n}} = 0, \end{aligned} \quad (\text{A.2})$$

$$\begin{aligned} & \frac{\sigma_{m+1,n} - \sigma_{m-1,n} + 2\tau_{y m,n} m_{\theta m,n}}{s_{\beta m+1,n} - s_{\beta m-1,n}} \left[1 + \sqrt{\frac{2}{3}} \varphi'_{\theta}(\delta_{\theta m,n}) \right] \frac{\delta_{\theta m+1,n} - \delta_{\theta m-1,n}}{s_{\beta m+1,n} - s_{\beta m-1,n}} + \\ & + \tau_{y m,n} \frac{m_{\theta m,n}}{\sqrt{3} \sqrt{1 - m_{\theta m,n}^2}} \text{sign}(\delta_{\theta m,n} - \delta_{\alpha m,n}) \frac{m_{\theta m+1,n} - m_{\theta m-1,n}}{s_{\beta m+1,n} - s_{\beta m-1,n}} + \\ & + \sqrt{3} \frac{\tau_{y m,n}}{r_{m,n}} \sqrt{1 - m_{\theta m,n}^2} \sin \delta_{\theta m,n} \text{sign}(\sigma_{\theta m,n} - \sigma_{\alpha m,n}) - \frac{\sqrt{1 - m_{\theta m,n}^2}}{\sqrt{3}} \text{sign}(\delta_{\theta m,n} - \delta_{\alpha m,n}) \frac{\tau_{y m+1,n} - \tau_{y m-1,n}}{s_{\beta m+1,n} - s_{\beta m-1,n}} + \\ & + \tau_{y m,n} \frac{m_{\theta m,n+1} - m_{\theta m,n-1}}{s_{\alpha m,n+1} - s_{\alpha m,n-1}} + \tau_{y m,n} \frac{m_{\theta m,n}}{r_{m,n}} \cos \delta_{\theta m,n} + m_{\theta m,n} \frac{\tau_{y m,n+1} - \tau_{y m,n-1}}{s_{\alpha m,n+1} - s_{\alpha m,n-1}} = 0, \end{aligned} \quad (\text{A.3})$$

$$\frac{v_{\alpha^* m,n+1} - v_{\alpha^* m,n-1}}{s_{\alpha m,n+1} - s_{\alpha m,n-1}} - v_{\beta^* m,n} \frac{\delta_{\theta m,n+1} - \delta_{\theta m,n-1}}{s_{\alpha m,n+1} - s_{\alpha m,n-1}} + \frac{v_{\alpha^* m,n} \cos \delta_{\theta m,n} - v_{\beta^* m,n} \sin \delta_{\theta m,n}}{2r_{m,n}} = 0, \quad (\text{A.4})$$

$$\frac{v_{\beta^* m+1,n} - v_{\beta^* m-1,n}}{s_{\beta m+1,n} - s_{\beta m-1,n}} + v_{\alpha^* m,n} \frac{\delta_{\theta m+1,n} - \delta_{\theta m-1,n}}{s_{\beta m+1,n} - s_{\beta m-1,n}} + \frac{v_{\alpha^* m,n} \cos \delta_{\theta m,n} - v_{\beta^* m,n} \sin \delta_{\theta m,n}}{2r_{m,n}} = 0, \quad (\text{A.5})$$

$$\frac{v_{\alpha^* m+1,n} - v_{\alpha^* m-1,n}}{s_{\beta m+1,n} - s_{\beta m-1,n}} - v_{\beta^* m,n} \frac{\delta_{\theta m+1,n} - \delta_{\theta m-1,n}}{s_{\beta m+1,n} - s_{\beta m-1,n}} = 0, \quad (\text{A.6})$$

$$\frac{v_{\beta^* m,n+1} - v_{\beta^* m,n-1}}{s_{\alpha m,n+1} - s_{\alpha m,n-1}} - v_{\alpha^* m,n} \frac{\delta_{\theta m,n+1} - \delta_{\theta m,n-1}}{s_{\alpha m,n+1} - s_{\alpha m,n-1}} = 0, \quad (\text{A.7})$$

where m,n denote indices m and n of the node points which are formed by intersection of the slip lines α_m and β_n (cf., Figure 7). For the initial approximate solution the additional condition (10) is expressed in a linear form for neighboring grid points of the plastic zone

$$\delta_{\theta m,n}^{(0)} = \delta_{\theta m-1,n}^{(0)} + \delta_{\theta m,n-1}^{(0)} - \delta_{\theta m-1,n-1}^{(0)}. \quad (\text{A.8})$$

A.2 Connection between the parameter m_θ and the Lode angle for the stresses, ϕ_σ , and strain rates, ϕ_ϵ

In context with the calculations of the stress and the plastic flow velocity fields a connection between the parameter m_θ and the Lode angle for the stresses, ϕ_σ , and strain rates, ϕ_ϵ , is used. The parametric form of Eqn. (17) for deviatoric stresses in the coordinates α , β becomes

$$s_\alpha = -\sqrt{\frac{2}{3}}\tau_y m_\beta \text{sign}(\sigma_\theta - \sigma_\alpha), \quad s_\beta = \sqrt{\frac{2}{3}}\tau_y m_\alpha \text{sign}(\sigma_\beta - \sigma_\theta), \quad (\text{A.9})$$

$$s_\theta = \sqrt{\frac{2}{3}}\tau_y [-m_\alpha \text{sign}(\sigma_\beta - \sigma_\theta) + m_\beta \text{sign}(\sigma_\theta - \sigma_\alpha)], \quad \tau_{\alpha\beta} = \tau_y m_\theta, \quad (\text{A.10})$$

or, if the sign functions during press forging are taken into account, *i.e.*, $\text{sign}(\sigma_\theta - \sigma_\alpha) = 1$, $\text{sign}(\sigma_\beta - \sigma_\theta) = -1$, we may write

$$s_\alpha = -\sqrt{\frac{2}{3}}\tau_y m_\beta, \quad s_\beta = -\sqrt{\frac{2}{3}}\tau_y m_\alpha, \quad s_\theta = \sqrt{\frac{2}{3}}\tau_y [m_\alpha + m_\beta], \quad \tau_{\alpha\beta} = \tau_y m_\theta. \quad (\text{A.11})$$

Similar relations are obtained for the deviatoric strain rates

$$\dot{\epsilon}_\alpha = -\sqrt{\frac{2}{3}}\dot{\epsilon} m_\beta, \quad \dot{\epsilon}_\beta = -\sqrt{\frac{2}{3}}\dot{\epsilon} m_\alpha, \quad \dot{\epsilon}_\theta = \sqrt{\frac{2}{3}}\dot{\epsilon} (m_\alpha + m_\beta), \quad \frac{1}{2}\dot{\gamma}_{\alpha\beta} = \dot{\epsilon} m_\theta. \quad (\text{A.12})$$

Since $m_\alpha = m_\beta = \sqrt{1 - m_\theta^2} / \sqrt{2}$, we obtain the following dependencies of the Lode angle ϕ_σ (or ϕ_ϵ) on the parameter m_θ (*cf.*, Figure A.1)

$$\cos(3\phi_\sigma) = -\frac{3\sqrt{3}I_3(s_{ij})}{2I_2^{3/2}(s_{ij})} = -(1 - 4m_\theta^2)\sqrt{1 - m_\theta^2}, \quad m_\theta \in \left[\frac{\sqrt{3}}{2}; 1\right]. \quad (\text{A.13})$$

The values $m_\theta = \sqrt{3}/2$ and $\phi_\sigma = 0$ correspond to uniaxial compression at the symmetry axis of the blank, while the values $m_\theta = 1$ and $\phi_\sigma = \pi/6$ correspond to pure shear ($\sigma_2 = (\sigma_1 + \sigma_3)/2$) in the outflow zone of the material into the radial clearance.

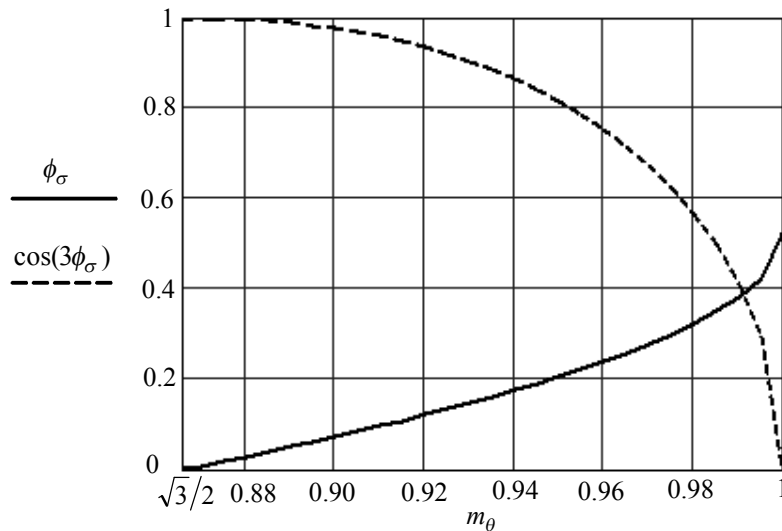


Figure A.1. Diagrams ϕ_σ vs. m_θ and $\cos(3\phi_\sigma)$ vs. m_θ .

Acknowledgements

The present work was supported by Deutsche Forschungsgemeinschaft (DFG) by a special program for funding research stays in Germany of researchers from Central and Eastern Europe/CIS.

References

- Bogatov, A.A.; Mizhiritskiy, O.I.; Smirnov, S.V.: *Resource of Metals Plasticity during Forming*. Moscow (1984) (in Russian).
- Chen, B.; Li, W.G.; Peng, X.H.: A microvoid evolution law involving change of void shape and micro/macroscale analysis for damaged materials. *J. Mater. Process. Techn.* 122, (2002), 189-195.
- Dung, N.L.: Plasticity theory of ductile fracture by void growth and coalescence. *Forsch. Ingenieurw.* 58, (1992), 135-140.
- Gurson, L., Continuum theory of ductile rupture by void nucleation and growth, *J. Eng. Mater. Technol., Trans. ASME* 99, (1977), 2-15.
- Hill, R.: *The Mathematical Theory of Plasticity*. Oxford Univ. Press (1950).
- Ilyushin, A.A.: *Plasticity: Fundamentals of the General Mathematical Theory*. Moscow (1963) (in Russian).
- Kachanov, L.M.: *Introduction to Continuum Damage Mechanics*. Kluwer Academic, (1986).
- Kachanov, L.M.: *Fundamentals of the Theory of Plasticity*. Dover Publications (2004).
- Korn, G.A.; Korn, T.M.: *Mathematical Handbook for Scientists and Engineers: Definitions, Theorems, and Formulas for Reference and Review*. 2nd revised edition, Dover Publications (2000).
- Krajcinovic, D.: Damage mechanics: accomplishments, trends and needs. *Int. J. Solids and Structures* 37, (2000), 267-277.
- Lemaitre, J.; Desmorat, R.: *Engineering Damage Mechanics: Ductile, Creep, Fatigue and Brittle Failures*. Springer (2007).
- Malmeisters, A.K.; Tamuzs, V.P.; Teters, G.A.: *Mechanik der Polymer werkstoffe*. Akademie-Verlag, Berlin (1977).
- McClintock, F.A.: A criterion for ductile fracture by the growth of holes. *J. Appl. Mech.* 90, (1968), 363-371.
- Rice, J.; Tracey, D.: On ductile enlargement of voids in triaxial stress field. *J. Mech. Phys. Solids* 17, (1969), 201-217.
- Sedov, L.I.: *Continuum Mechanics. Vol. 1*. Nauka, Moscow (1983) (in Russian).
- Thomson, E.; Young, C.; Kobayashi, S.: *Mechanics of Plastic Strains in Metalworking* (1968).
- Tutyshkin, N.D.: Metal plastic straining processes with predictable mechanical and constitutive properties modeling. *IASME Trans.* 9, (2005), 1819-1825.
- Tutyshkin, N.D.; Gvozdev, A.E.; Tregubov, V.I.; Poltavets, Y.V.; Selyodkin, E.M.; Pustovgar, A.S.: *Complex Problems of the Plasticity Theory*. Tulskiy Polygraphist, Tula (2001) (in Russian).
- Unksov, E. P.; Johnson, W.; Kolmogorov, V. L.: *Theory of plastic deformation of metals*, by E. P. Unksov and A. G. Ovchinnikov (eds.), Mashinostroenie, Moscow (1992) (in Russian).

Voyiadjis, G.Z.; Kattan, P.I.: *Advances in Damage Mechanics: Metals and Metal Matrix Composites with an Introduction to Fabric Tensors*. 2nd Edition. Elsevier (2006).

Yokobori, T.: *An Interdisciplinary Approach to Fracture and Strength of Solids*. Gordon & Breach, Pub. New York (1968).

Zapara, M.A.; Tutyshkin, N.D.; Müller, W. H.; Weinberg, K.; Wille, R.: A physico-mechanical approach to modeling of metal forming processes – part I: theoretical framework. *Continuum Mech. Thermodyn.* 20, (2008), 231-254

Addresses: Dr. M.A. Zapara and Prof. Dr. N.D. Tutyshkin, Department of Technological Mechanics, Tula State University, 300600 Tula, Russia. email: tutyshkin@mail.ru
Prof. Dr. W.H. Müller and Dr. R. Wille, Lehrstuhl für Kontinuumsmechanik und Materialtheorie, Technische Universität Berlin, Sekretariat MS 02, Einsteinufer 5, D-10587 Berlin, Deutschland.
email: Wolfgang.H.Mueller@tu-berlin.de, Ralf.Wille@tu-berlin.de